Evaluation of Polar MM5 simulations of Greenland's atmospheric circulation

John J. Cassano,[1,2] Jason E. Box,[3] David H. Bromwich,[1,4] Lin Li,[1,4] and Konrad Steffen[3]

Abstract. A complete annual cycle over the Greenland ice sheet is simulated with the Polar MM5, a mesoscale model optimized for use over extensive ice sheets. These simulations are compiled from a series of short duration (48 hour), forecast mode, simulations. The model output is compared to observations primarily from the Greenland Climate Network automatic weather station (AWS) array. The model simulations show a high degree of skill for all variables evaluated with the AWS data (pressure, temperature, water vapor mixing ratio, wind speed and direction, downwelling shortwave radiation, and net radiation) for all seasons, although the use of a fixed albedo in the Polar MM5 leads to large errors in the simulated net radiation budget over melting ice surfaces during the summer months. The modeled precipitation distribution agrees with available observations in the interior of the ice sheet but is excessive along the steep margins of the island. A discussion of possible future applications of the Polar MM5 is presented.

1. Introduction

A few years ago it could be said that the Greenland ice sheet was one of the least explored areas of the Northern Hemisphere from a meteorological perspective [Bromwich et al., 1993]. The 1990s have seen an explosion of interest in the Greenland atmospheric circulation. Most notable is the establishment of the climate network of automatic weather stations (AWS) across the ice sheet (GC-NET described in section 3 [Steffen et al., 1996]) to complement that established earlier around Summit in support of the deep ice core drilling [Stearns et al., 1997]. Observations of the katabatic circulation and boundary layer structure over Greenland, using AWS and instrumented aircraft, were conducted during the Katabatic Wind and Boundary Layer Front Experiment Around Greenland during 1997 (KABEG'97) [Heinemann, 1999]. Extensive investigations have been carried out on the mass balance of the ablation zone during the Greenland Ice Margin Experiment (GIMEX) [Oerlemans and Vugts, 1993]. Complementary studies have been conducted to understand the variability of snow accumulation over the ice sheet interior and its relationship to modes of the large-scale atmospheric circulation [Chen et al., 1997; Bromwich et al., 1999; McConnell et al., 2000].

Numerical modeling has been widely used to complement the above observational and diagnostic investigations. A key application of numerical models has been to understand the governing atmospheric processes such as those that determine ablation [Meesters, 1994; Gallée and Duynkerke, 1997], barrier wind formation [van den Broeke and Gallée, 1996], and katabatic wind dynamics [Bromwich et al., 1996; Heinemann, 1999]. Most of these detailed numerical investigations have been in two dimensions, along the ice slope and perpendicular to it. Limited efforts have been made to use atmospheric models to provide a more comprehensive three-dimensional description of the atmosphere for the entire ice sheet than is possible from the scattered observations concentrated in the coastal margins [Bromwich et al., 1996; Bromwich et al., 2001; T. Klein et al., Mesoscale modeling of katabatic winds over Greenland: Comparison of NORLAM simulations with AWS and aircraft data, submitted to Meteorology and Atmospheric Physics, 2001]. For example, Bromwich et al. [1996] used an idealized atmospheric model to establish the typical characteristics of the downslope surface (katabatic) winds during winter.

Models provide an ideal environment for testing the importance of critical processes in a controlled fashion; the sensitivity of ice sheet precipitation to adjacent oceanic conditions is a good example of this application. Ohmura et al. [1996] and Thompson and Pollard [1997] have presented simulations of the mass balance of the ice sheet and its sensitivity to climate change using global climate models (GCMs). A key concern with this type of research is how to apply the results to the narrow (10-20 km wide) ablation zone. One solution to this problem is to embed a regional model, such as examined here, within the GCM to provide high resolution of the topographic forcing. Another potentially important model application is numerical weather prediction in support of field parties on the ice sheet. For any of these model applications it is an essential prerequisite that the model skill is determined through detailed comparison with available observations.

Here a detailed assessment is presented of the performance of a regional atmospheric model adapted specifically for ice sheet environments. The numerical model that is verified is

---

[1]Polar Meteorology Group, Byrd Polar Research Center, The Ohio State University, Columbus, Ohio, USA.
[2]Now at Cooperative Institute for Research in Environmental Sciences, University of Colorado, Boulder, Colorado, USA.
[3]Cooperative Institute for Research in Environmental Sciences, University of Colorado, Boulder, Colorado, USA.
[4]Also at Atmospheric Sciences Program, Department of Geography, The Ohio State University, Columbus, Ohio.

based on the Pennsylvania State University (PSU)/National Center for Atmospheric Research (NCAR) fifth-generation mesoscale model (MM5), a widely used and publicly available regional atmospheric model [*Grell et al.,* 1994] with a full range of sophisticated capabilities. Section 2 describes the modifications to this model, referred to as the Polar MM5, which are required to make it suitable for ice sheet environments, in general, and Greenland, in particular.

The Polar MM5 has been run for the period of April 1997 through March 1998 in a yearlong series of short-term forecasts (referred to as forecast mode simulations) from initial and boundary conditions provided by the operational analyses of the European Centre for Medium-Range Weather Forecasts (ECMWF). This 12 month period was selected to provide a test of the model performance over an entire annual cycle, to provide overlap with the KABEG'97 field experiment [*Heinemann,* 1999], and to contain a period when a significant amount of data from the GC-NET AWS was available (14 AWS sites were operational during this 12 month period). The North Atlantic Oscillation (NAO), which represents the dominant mode of atmospheric variability in the North Atlantic and Greenland region [*van Loon and Rogers,* 1978; *Hurrell,* 1995], for April 1997 through March 1998 is slightly negative relative to the long-term average and does not represent an extreme NAO anomaly.

The model skill, primarily in relation to near-surface observations from the GC-NET AWS sites (described in section 3), is evaluated in section 4 on synoptic and diurnal timescales, with a discussion of the model performance throughout the entire annual cycle. Additional evaluation of the Polar MM5, using the data from the KABEG'97 field campaign is presented by *Bromwich et al.* [2001]. Concluding remarks on the model performance and possible future applications of the Polar MM5 to problems associated with ice sheet meteorology, such as those discussed above, are given in section 5.

2. Polar MM5

The Polar MM5 model is based on version 2 of the PSU/NCAR MM5. A general description of version 2 of MM5 is given by *Dudhia* [1993] and *Grell et al.* [1994]. The model configuration used for the simulations presented in this paper is described below. In addition, a description of the changes made to the standard version of MM5 for use in polar regions is provided.

2.1. Polar MM5 Dynamics and Physics

The standard version of MM5 (version 2) allows for the use of either hydrostatic or nonhydrostatic governing dynamics. For the Greenland simulations presented in this paper the hydrostatic dynamics option is used because the hydrostatic approximation is valid for the model horizontal grid spacing used (40 km), and the hydrostatic option was found to run approximately 12% faster than the nonhydrostatic option. The hydrostatic version of the model includes three-dimensional prognostic equations for the horizontal components of the wind and temperature, and a two-dimensional prognostic equation for p^* (defined as the surface pressure minus the pressure at the model top). Additional three-dimensional prognostic equations for the water vapor mixing ratio and the mixing ratio of various cloud species are also part of the model equations. Parameterizations for cloud microphysics and precipitation processes, cumulus convection, radiative transfer, and turbulence are included in the model, with multiple options available for the representation of many of these processes.

For the Polar MM5 simulations the large-scale (grid) cloud and precipitation processes are represented by the Reisner explicit microphysics parameterization [*Reisner et al.,* 1998]. This parameterization predicts the mixing ratio of cloud water and ice crystals as well as the rain and snow water mixing ratios. Sub-grid scale clouds are parameterized with the Grell cumulus parameterization [*Grell et al.,* 1994].

Excessive cloud cover was found to be a problem over the Antarctic in sensitivity simulations using an older version of MM5 (MM4) [*Hines et al.,* 1997a, 1997b], similar to results found by *Manning and Davis* [1997] for cold, high clouds over the continental United States. Replacement of the *Fletcher* [1962] equation for ice nuclei concentration with that of *Meyers et al.* [1992] in the MM5 explicit microphysics parameterizations, as suggested by *Manning and Davis* [1997], helped to eliminate this cloudy bias in polar simulations with MM5 and is now a standard option in the Polar MM5 model. This modification to the Reisner microphysics parameterization is used for all of the simulations presented here.

The Polar MM5 also uses a modified version of the NCAR community climate model, version 2, (CCM2) radiation parameterization [*Hack et al.,* 1993] for prediction of the radiative transfer of shortwave and longwave radiation through the atmosphere. In the original version of this parameterization the cloud cover was predicted as a simple function of the grid box relative humidity, with the cloud liquid water (CLW) path determined from the grid box temperature. Sensitivity simulations revealed that this parameterization of cloud cover tended to significantly overestimate the CLW path, and thus the radiative effects of the clouds, which was particularly noticeable as large downwelling longwave radiation fluxes during the austral winter over the Antarctic ice sheet [*Hines et al.,* 1997a, 1997b]. To resolve this problem, the predicted cloud water and ice mixing ratios from the Reisner explicit microphysics parameterization are used in the modified CCM2 radiation parameterization for determination of the radiative properties of the modeled cloud cover. This modification allows for a consistent treatment of the radiative and microphysical properties of the clouds and for the separate treatment of the radiative properties of liquid and ice phase cloud particles, similar to that in the CCM3 radiation parameterization [*Kiehl et al.,* 1996] which is in part based on the results of *Ebert and Curry* [1992]. It should be noted that this method treats cloud particles as equivalent spheres and has been shown to be inaccurate for nonspherical ice particles [*Grenfell and Warren,* 1999].

Turbulent fluxes in the atmosphere, and the turbulent fluxes between the atmosphere and the surface, are parameterized using the 1.5-order turbulence closure parameterization used in the National Centers for Environmental Prediction Eta model [*Janjić,* 1994]. Heat transfer through the model substrate is predicted using a multilayer "soil" model. The thermal properties used in the "soil" model for snow and ice surface types are modified following *Yen* [1981]. In addition, the number of substrate levels represented in the "soil" model is increased from 6 to 8, with an increase in the resolved substrate depth from 0.47 m to 1.91 m. Also, a sea ice surface type is added to the 13

Table 1. List of Data Sets and Initial Settings Used for Polar MM5 Simulations

	Input Data
Initial and boundary condition atmospheric data	12 hourly 2.5° ECMWF TOGA global analyses
Topography	*Ekholm* [1996], 2 km resolution
Sea surface temperature	6 hourly 1.125° ECMWF TOGA global surface analyses
Sea ice coverage	Sea ice surface type for ocean grid points with SST < 271.7 K, sea ice fraction based on climatological values [*Gloersen et al.,* 1992]

Surface Type	Albedo	Roughness Length (m)
Ice sheet	0.80	1×10^{-4}
Tundra (summer)	0.15	0.1
Tundra (winter)	0.70	0.1
Sea ice	0.70	1×10^{-3}
Ocean	0.15	minimum 1×10^{-4} with Charnock relation

surface types available in the standard version of MM5 [*Hines et al.,* 1997a]. The sea ice surface type allows for the specification of fractional sea ice cover in the model initial conditions for any oceanic grid point, and this sea ice distribution does not evolve during the model simulation. The surface fluxes for the sea ice grid points are calculated separately for the open water and sea ice portions of the grid point, and these fluxes are then averaged before interacting with the overlying atmosphere. The sea ice thickness varies from 0.2 m to 0.95 m and is dependent on the hemisphere and sea ice fraction at the grid point. Some surface characteristics

for the surface types of interest in this study are listed in Table 1.

2.2. Model Grid

MM5 is formulated using a staggered horizontal grid with a vertical σ-coordinate system that is defined in terms of pressure. The model domain used in this study consists of 100 grid points in the north/south direction and 110 grid points in the east/west direction, centered at 71°N latitude and 30°W longitude, with a horizontal grid spacing of 40 km (Figure 1). This grid spacing adequately resolves the terrain over all but
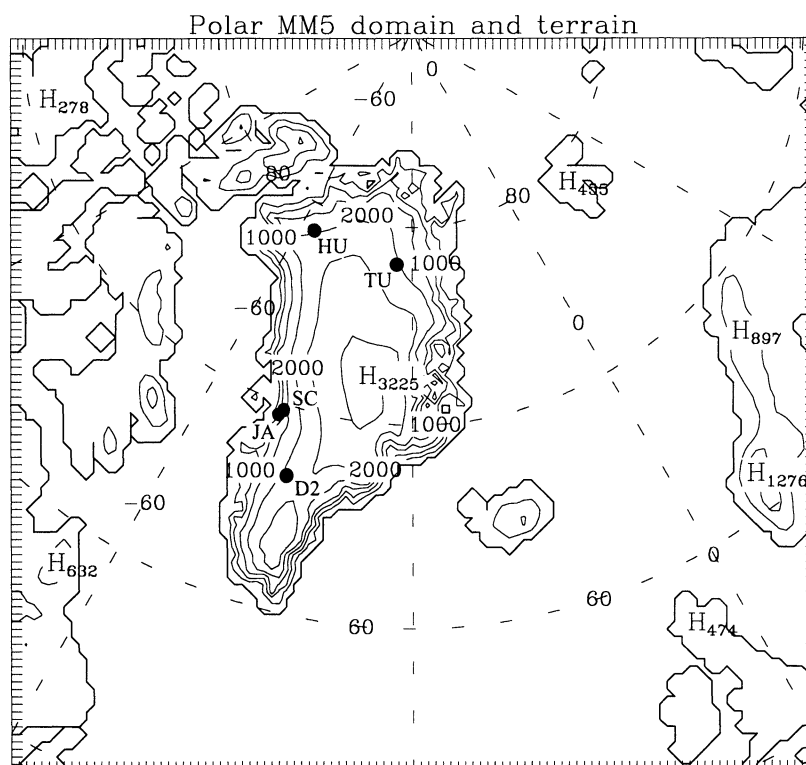
Figure 1. Polar MM5 model domain and terrain. Elevation contour interval is 500 m. The location of the GC-NET AWS sites DYE-2 (D2), JAR 1 (JA), Swiss Camp (SC), Humboldt (HU), and Tunu-N (TU) are indicated with solid circles.

the steepest margins of the ice sheet [*Cassano and Parish*, 2000]. A total of 28 σ levels are used, of which seven are located within the lowest 400 m of the atmosphere. The lowest sigma level is located at a nominal height of 12 m above ground level (agl). The use of higher resolution near the surface is required to accurately represent the evolution of the shallow katabatic layer over the Greenland ice sheet. The model top is set at a constant pressure of 100 hPa.

2.3. Polar MM5 Initial and Boundary Condition Data

A list of the data sets used to initialize the Polar MM5 and which are used to provide boundary conditions to the model during the simulations are listed in Table 1. The 2.5° ECMWF Tropical Ocean–Global Atmosphere (TOGA) surface and upper air operational analyses are used to provide the initial and boundary conditions for the model atmosphere. These data are interpolated to the Polar MM5 model grid using the standard preprocessing programs provided by NCAR for use with the MM5 modeling system. In addition, the 1.125° ECMWF TOGA global surface analyses are used to specify the initial surface temperature (and sea surface temperature (SST)), deep soil temperature, and snow cover. Snow cover on the tundra grid points on Greenland is manually specified to match snow cover observations from the KABEG'97 field campaign. Sea ice cover is based on the SST specified with the higher-resolution surface data and is considered to be present at all grid points with a SST < 271.7 K. Sea ice fraction for these grid points is determined on the basis of climatological values given by *Gloersen et al.* [1992]. Sea ice cover determined in this manner compares favorably with remotely sensed sea ice cover observations. The surface temperature, SST, deep soil temperature, snow cover, and sea ice cover are updated in the model initial conditions for each forecast mode simulation.

The Polar MM5 is used to produce short duration (48 hour length) simulations of the atmospheric state over Greenland from April 1997 to March 1998. (These short simulations are referred to as "forecast mode" simulations because they are of a similar duration to many operational numerical weather prediction forecasts.) The model is initialized with the 0000 UTC ECMWF analyses for each day of this 12 month period, with the 24 – 48 hour forecast used for the model evaluation.

3. GC-NET AWS Data

The primary data source used for evaluation of the Polar MM5 simulations presented in this paper is the observations from the GC-NET AWSs [*Steffen et al.*, 1996]. The GC-NET is part of the Program for Arctic Regional Climate Assessment (PARCA) and as of August 1999 contained 18 AWSs. Locations of the AWS sites referred to in this study are shown in Figure 1. A location map of all of the GC-NET AWS sites is given by *Steffen and Box* [this issue]. During the model evaluation period (April 1997 through March 1998), 14 AWS sites were operational (Table 2), although not all of these sites contain complete records during this period.

The GC-NET AWSs measure air temperature, relative humidity, wind speed and direction, and elevation to the snow surface at two measurement heights (typically between 1 and 4 m agl). The air temperature is measured using two different instruments at each measurement height, for a total of four air temperature measurements at each AWS site. The AWSs also measure downwelling and upwelling shortwave radiation, net radiation, and air pressure. Measurements of the snow temperature at ten depths are also made at each AWS site.

A list of the instruments used to make the measurements at the AWS and the instrument accuracy are given in Table 3. All of the AWS observations were quality controlled and error checked prior to use for model evaluation. A visual inspection of time series of net radiation measurements indicates periods with minimum net radiation during daylight hours and/or prolonged periods of nearly constant, zero, net radiation at AWS sites located above 1100 m. These problems are probably caused by hoarfrost formation on the radiometer domes. As a result of these problems, evaluation of the modeled net radiation budget is restricted to the JAR 1 AWS site (Table 2). (Visual inspection of the shortwave radiation measurements does not reveal similar problems, and the shortwave radiation measurements from all AWS sites are used for the evaluation of the Polar MM5 simulations). All other AWS measurements are assumed to be accurate to within the limits specified in Table 3, based on the extensive quality control procedures applied to these data.

The temperature and wind speed predicted by the Polar MM5 is interpolated from the model lowest level (nominal 12

Table 2. Latitude, Longitude, and Elevation of GC-NET AWS Sites Operational During April 1997 Through March 1998

Station Name	Latitude (°N)	Longitude (°W)	Elevation (m)
Swiss Camp	69.57	49.32	1149
Crawford Point 1	69.88	46.99	2022
NASA-U	73.84	49.50	2369[a]
GITS	77.14	61.04	1887
Humboldt	78.53	56.83	1995[a]
Summit	72.58	38.50	3254
Tunu-N	78.02	33.99	2113[a]
DYE-2	66.48	46.28	2165
JAR 1	69.50	49.68	962[a]
Saddle	66.00	44.50	2559
South Dome	63.15	44.82	2922
NASA-E	75.00	30.00	2631
Crawford Point 2	69.88	46.99	1990
NGRIP	75.10	42.33	2950

[a]Elevation determined using differential GPS measurement.

Table 3. GC-NET AWS Instrumentation and Instrument Accuracy

Parameter	Instrument	Instrument Accuracy
Air temperature	Campbell Scientific CS-500	0.1° C
Air temperature	Type-E thermocouple	0.1° C
Relative humidity (RH)	Campbell Scientific CS-500	5% for RH < 90%
		10% for RH > 90%
Wind speed	RM Young propeller-type vane	0.1 m s^{-1}
Wind direction	RM Young propeller-type vane	5°
Station pressure	Vaisala PTB101B	0.1 hPa
Shortwave radiation flux	Li-Cor Photodiode	5-15%
Net radiation	REBS Q*7	5-50%

m agl) to a constant height of 2 m agl for comparison with the AWS measurements. This interpolation is done by applying Monin-Obukhov similarity theory [*Stull*, 1988] to the temperature and wind speed at the lowest model level, the model surface temperature, and the model-specified surface roughness length. In applying this interpolation the diabatic correction term from the Monin-Obukhov similarity theory is neglected, given the problems with similarity theory for very stable surface layers. The model surface pressure has also been adjusted from the model grid point elevation to the elevation of the AWS observation, using the hypsometric equation. The elevation of the AWS sites is known to within ±20 m, based on handheld global positioning system (GPS) measurements, and this introduces an uncertainty in the elevation-adjusted model pressure of ±2 hPa. The elevation of certain AWS sites is determined using differential GPS measurements and are known to an accuracy of ±0.1 m (see Table 2 for a list of these sites). All other model output is not modified prior to comparison with the AWS observations.

4. Evaluation of Polar MM5 Simulations

Model output from the Polar MM5 simulations over the Greenland ice sheet is compared to available observational data on annual, seasonal, synoptic, and diurnal timescales in the following sections. This comparison is intended to demonstrate the high level of skill present in the Polar MM5 simulations over diurnal to synoptic timescales for all seasons. This analysis also serves to highlight areas requiring additional model improvements.

4.1. Annual Mean

Annual mean fields from the Polar MM5 simulations are calculated for the near-surface air temperature, near surface winds, and accumulated precipitation. These model fields are compared with available data in the discussion below.
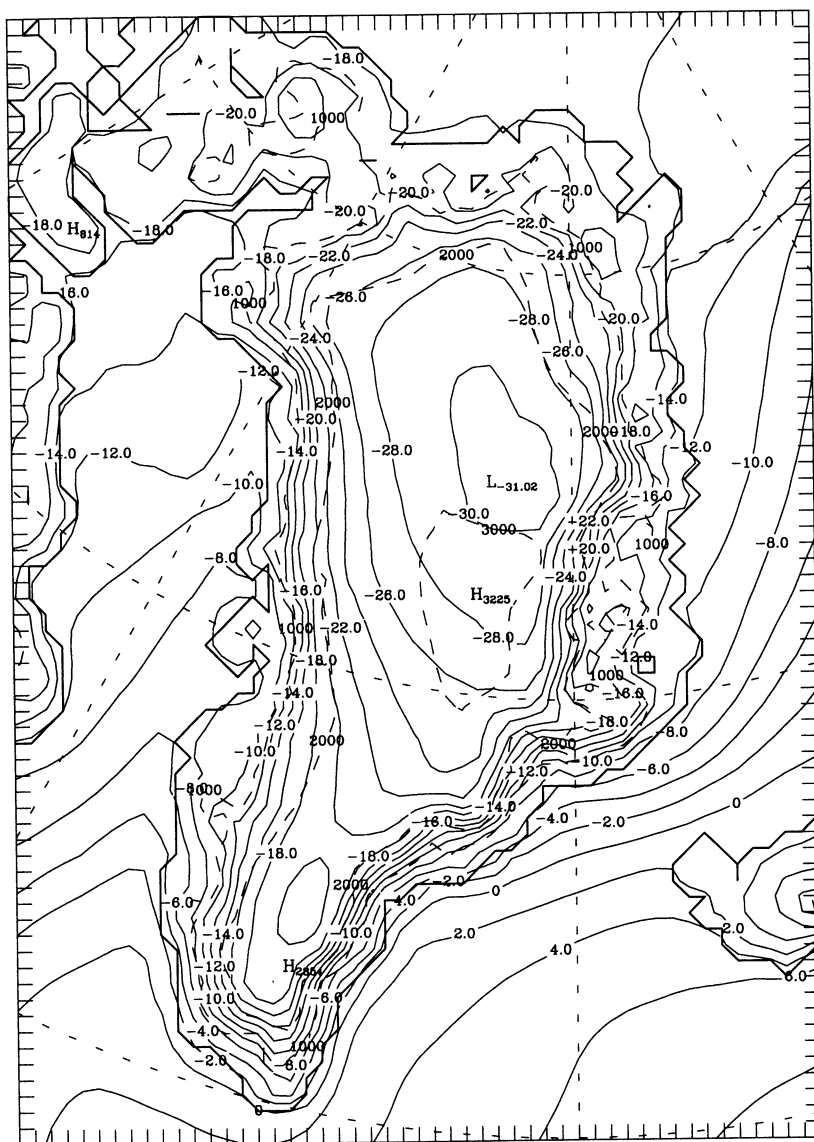
The Polar MM5 mean annual surface temperature is shown in Figure 2. The model-predicted mean annual surface temperature distribution is similar to the 5 year mean given by *Steffen and Box* [this issue] for 1995-1999. The coldest temperatures from the model are located north and east of the highest elevations of the ice sheet, in a region of time-mean subsidence [*Chen et al.*, 1997] and reduced cloud cover (not shown), while *Steffen and Box* [this issue] show that the coldest mean annual temperatures are located near Summit and along the ice divide that extends north of the summit of Greenland. A second minimum in temperature is found near

the highest terrain of southern Greenland for both the Polar MM5 simulations and the Steffen and Box analysis. Differences between the Steffen and Box compilation of the mean annual surface temperature and the modeled mean annual surface temperature may, in part, be caused by interannual variability not represented in the single annual cycle simulated by the Polar MM5. Despite this possible source of difference between the Steffen and Box data set and the Polar MM5 output, there is a high degree of similarity. As will be shown below, the model reproduces the annual cycle of temperature quite accurately at a large number of AWS sites located on the Greenland ice sheet, lending further credence to the distribution of the mean annual temperature simulated by the Polar MM5.

The Polar MM5 annual resultant wind vectors and wind speeds, from the lowest model level (approximately 12 m agl), are shown in Figure 3. The wind over the ice sheet is directed downslope and to the right of the ice fall line, as expected for katabatic flow in the Northern Hemisphere. The weakest resultant wind speeds are located along the ice divide, with stronger flow located in regions of steeper terrain slope, where the most persistent katabatic flow is likely to be located. The Polar MM5-simulated resultant annual wind field is similar to the idealized, clear-sky wintertime simulations over Greenland presented by *Bromwich et al.* [1996], using the *Parish and Waight* [1987] mesoscale model. The primary difference between the simulations is the larger cross-slope flow simulated by the Polar MM5. This larger cross-slope wind component is probably caused by a combination of cloud cover and the inclusion of summertime conditions in the Polar MM5 average. Both of these factors will reduce the near-surface temperature inversion, weaken the katabatic flow, and lead to enhanced cross-slope flow.

The total precipitation from the Polar MM5 and from the *Chen et al.* [1997] (see also D.H. Bromwich et al. (unpublished data, 2001)) dynamic precipitation retrieval method for April 1997 through March 1998 are shown in Figures 4a and 4b, respectively. The Polar MM5-predicted precipitation over all of Greenland is forecast by the model explicit microphysics parameterization (i.e., resolved scale precipitation), with only a very small contribution from the model convective parameterization along the southern coastal regions of Greenland and over the ocean. This is consistent with the expectation that large-scale, synoptically driven precipitation events, rather than convective precipitation events, are dominant over Greenland.

The total precipitation from the Polar MM5 shows

Figure 2. Mean annual surface temperature from Polar MM5. Mean annual temperature is contoured as solid lines, with a contour interval of 2°C. Terrain elevation is contoured with dashed lines and a contour interval of 1000 m.

increased mesoscale detail compared to the Chen et al. distribution, although both precipitation distributions are qualitatively similar. In general, the Polar MM5 precipitation exceeds that diagnosed with the Chen et al. method, with the greatest differences located along the coasts and steep margins of the ice sheet. Figures 4a and 4b both indicate a minimum of precipitation in north central Greenland. In both models, smaller annual precipitation totals are predicted along the highest ice sheet elevations in central and southern Greenland, with larger values near the coast. The maximum annual precipitation in the Polar MM5 is located on the southeast coast of Greenland, with a value in excess of 400 cm yr^{-1}. The Chen et al. diagnosed precipitation also has a maximum value on the southeast coast of Greenland, with a value of nearly 120 cm yr^{-1}. The excessive precipitation predicted by the Polar MM5 along the steep margins of the Greenland ice sheet is similar to a problem documented by *Colle et al.* [1999] for operational forecasts along the steep

windward slopes of the Cascade Mountains of the northwestern United States, and the source of this error needs further analysis.

4.2. Seasonal Cycle

The monthly mean values of surface pressure, temperature, water vapor mixing ratio, and wind speed are averaged over the five AWS sites (DYE-2, JAR 1, Swiss Camp, Humboldt, and Tunu-N; see Figure 1 for location of AWS sites) which had nearly complete records of all variables from April 1997 to March 1998 and the corresponding model grid points in the Polar MM5. These monthly means are plotted in Figure 5.

The monthly bias, root-mean-square error (RMSE), and correlation coefficient from the comparison of the Polar MM5 simulations to the AWS observations are also calculated from the 3 hourly AWS observations and model output. (It should be noted that the AWS data are available as hourly data, but the model output is archived at 3 hour intervals only). The
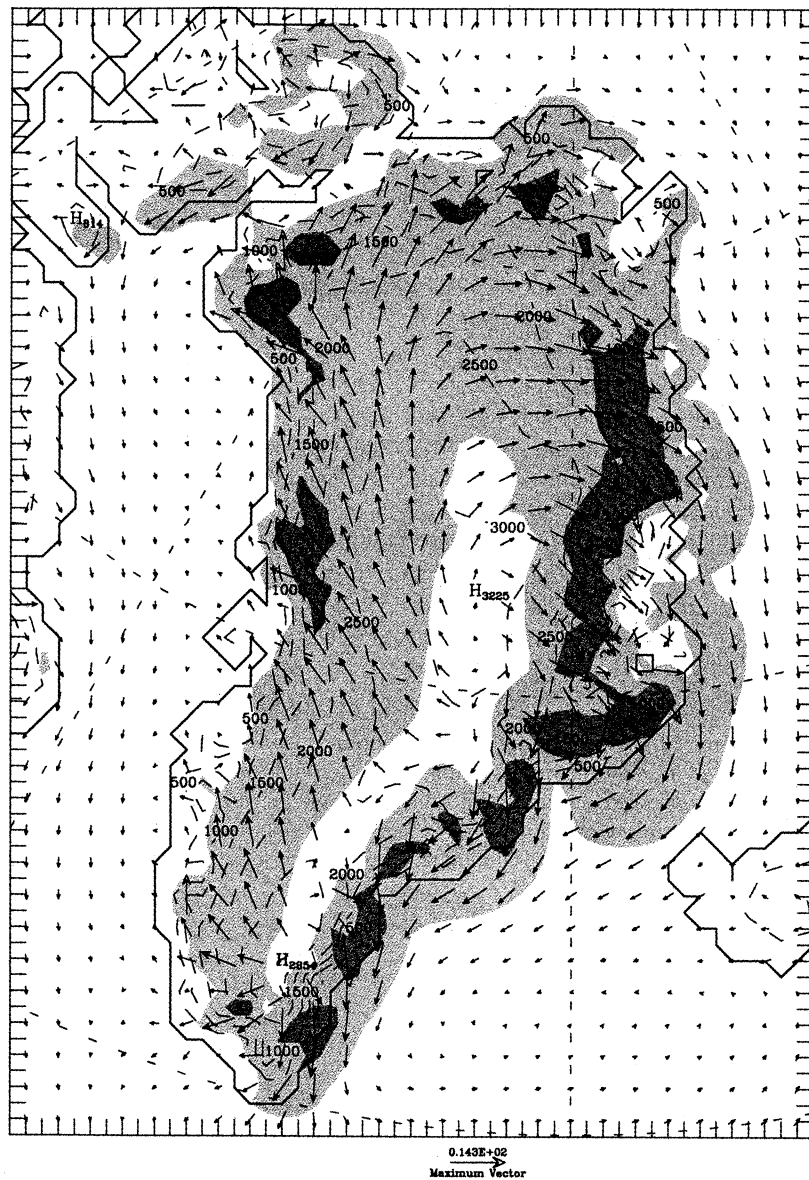
Figure 3. Polar MM5 annual resultant wind vectors, resultant wind speed, and terrain elevation contours. The resultant wind speed is indicated by gray shading (unshaded < 5 m s^{-1}, light gray 5 to 10 m s^{-1}, dark gray > 10 m s^{-1}). Terrain elevation is contoured with dashed lines and a contour interval of 500 m.

bias is defined as the difference between the Polar MM5 monthly mean and the AWS observed monthly mean value of a given variable and identifies any systematic differences between the Polar MM5 simulation and the AWS observations. The RMSE is calculated as the square root of the monthly averaged squared difference between the AWS observation and the Polar MM5-simulated value of a given variable, and is a measure of the "typical" difference between the Polar MM5-simulated and the AWS-observed values. It should be noted that the RMSE is influenced by large differences between the two data sets due to the squared difference term. The correlation coefficient measures the agreement in the phase of the variations in the modeled and observed time series. These three model verification statistics, averaged over the same five sites as in Figure 5, are shown in Figure 6. Table 4 lists the maximum and minimum monthly bias, RMSE, and correlation coefficient averaged over the

five AWS sites listed above, averaged over all of the GC-NET AWS sites, and at the individual AWS sites of DYE-2, JAR 1, Swiss Camp, Humboldt, and Tunu-N for the entire 12 month period for each variable. From Figures 5 and 6 and Table 4 it is evident that the forecast mode Polar MM5 simulations accurately represent the short-term atmospheric evolution for all seasons over the Greenland ice sheet. The model performance for each of the near-surface variables is discussed below.

In general, the model-simulated pressure, temperature, mixing ratio, and wind speed all have small monthly biases relative to the AWS observations. The bias in the modeled pressure, averaged over the five AWS sites is negative throughout the entire annual cycle (-3.4 to -0.5 hPa), with the largest magnitude bias during the summer months and the smallest magnitude bias during the winter months. The monthly mean temperature and mixing ratio simulated by the

(a) annual precipitation from Polar MM5
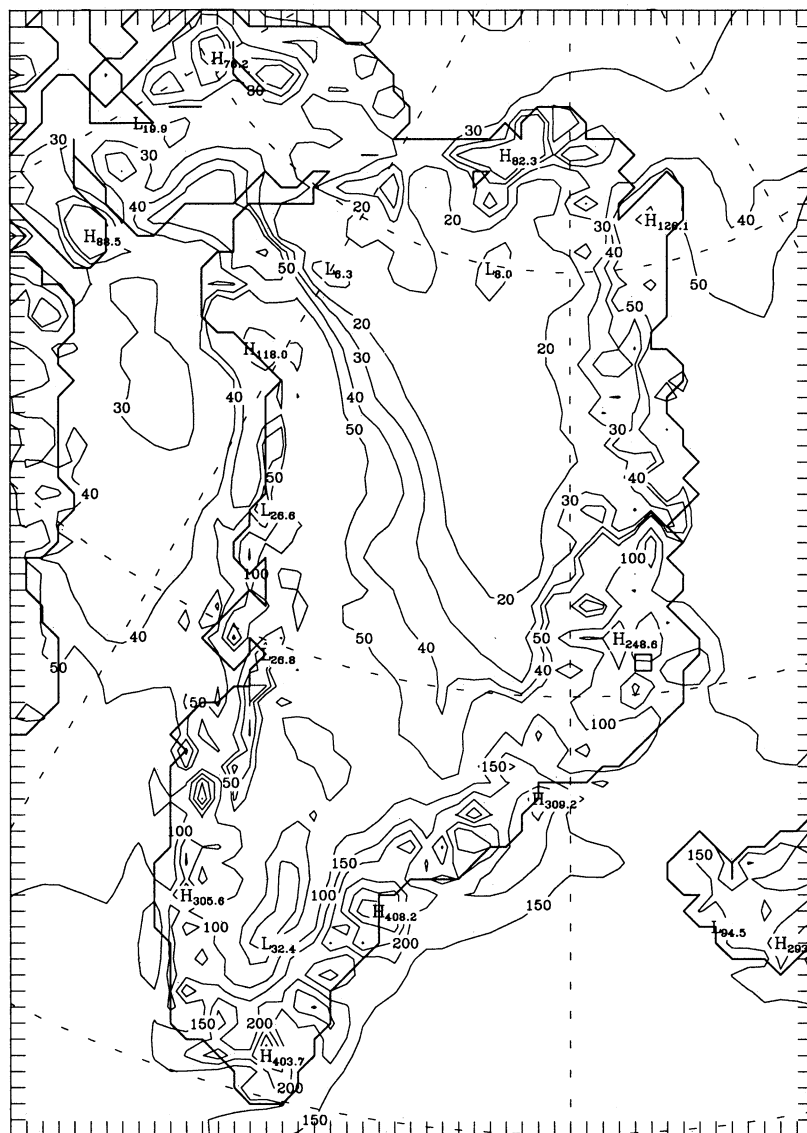
Figure 4. Annual precipitation simulated by the Polar MM5 (a) and the Chen et al. [1997] dynamic precipitation retrieval method (b) for April 1997 through March 1998. For Figure 4a the contour interval is 10 cm for precipitation amounts less than 50 cm and is 50 cm for precipitation amounts greater than 50 cm. In Figure 4b the contour interval is 10 cm for precipitation amounts less than 60 cm and is 20 cm for precipitation amounts greater than 60 cm.

Polar MM5 are less than observed throughout most of the annual cycle (-1.5° to 0.8°C and -0.29 to 0.12 g kg^{-1}, respectively), with the largest differences occurring during the late summer through winter months. The modeled monthly mean wind speeds are similar to the observations during the spring and summer months, with a positive bias during the late summer through winter months.

The negative bias in the modeled pressure, averaged over the five AWS sites, is caused in part by the large negative bias present at the Tunu-N AWS site (Table 4). Given the generally good agreement between the Polar MM5 simulations and the observations for other variables at Tunu-N (as will be shown below), and the realistic distribution of the surface winds shown in Figure 3, it is possible that the

large bias at Tunu-N is the result of an instrument error rather than a model error (the calibration of the pressure sensor at the Tunu-N AWS site will be verified during an upcoming field season). In contrast, the seasonal variations in the pressure bias of the Polar MM5 (larger negative biases during the summer months and smaller negative biases during the winter months) probably reflect model errors. During the winter months, when the Polar MM5 temperature bias is most negative, the modeled surface pressure bias becomes less negative consistent with a hydrostatic increase in the model surface pressure in response to the colder atmosphere.

The seasonal distribution of the bias of other model variables also exhibit similar physically consistent links. The similarity in the monthly distribution of the bias in the

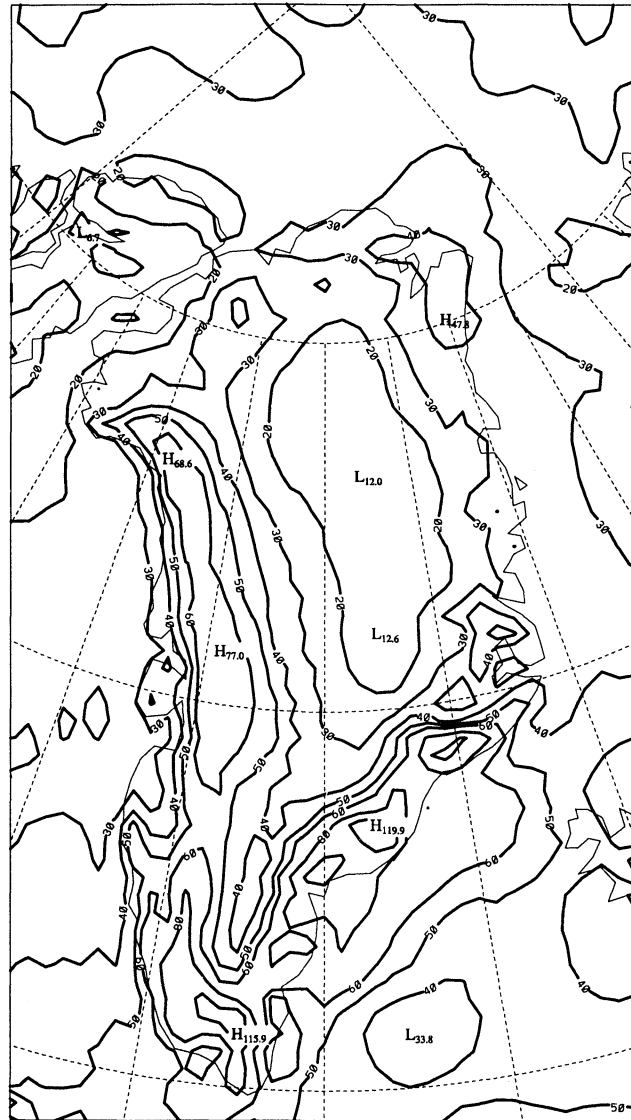**(b) annual precipitation from Chen et al. method**

Figure 4. (continued)

modeled temperature and mixing ratio is caused by the strong dependence of the atmospheric moisture content on the air temperature. The cold bias in the model implies a reduced capacity of the model atmosphere to hold water vapor and leads to the negative bias in the modeled mixing ratio. The period of positive wind speed bias corresponds to the time period with the largest negative temperature bias and is thought to be caused by enhanced drainage flow forced by the colder near-surface air in the model. It can be seen that the model bias in one variable is linked to biases in other variables, in a physically consistent manner.

The correlation between the modeled and the observed monthly time series tends to be largest for the surface pressure (0.95 to 0.99) and smallest for the wind speed (0.62 to 0.75), with intermediate values for the temperature (0.73 to 0.95) and mixing ratio (0.69 to 0.91). The large values of the correlation coefficient for these variables are indicative of the accurate timing of changes in the modeled near-surface atmospheric state.

The RMSE for the pressure and wind speed exhibit little seasonal variation (3 to 4 hPa and 2 to 3 m s^{-1}, respectively), while the temperature and water vapor RMSE vary more during the annual cycle (2° to 4.5°C and 0.13 to 0.63 g kg^{-1}, respectively). The temperature RMSE is largest during the synoptically active winter months and smallest during the summer months. The opposite pattern holds for the mixing ratio, but in this case, the reduced RMSE during the winter months reflects the smaller magnitude of the mixing ratio during the cold season and not an increase in model skill for this variable. In fact, the ratio of the RMSE to the mean mixing ratio (the relative RMSE) is smallest during the summer months and largest during the winter months, similar to the seasonal distribution of the temperature RMSE. The less skillful prediction of the temperature and water vapor mixing ratio during the winter months is caused by small errors in the timing of some synoptic disturbances in the model, which cause large errors in the modeled temperature and mixing ratio.

The modeled surface radiation budget is evaluated using the available GC-NET radiation measurements. The monthly mean downwelling shortwave radiation and the calculated bias, RMSE, and correlation coefficient, all averaged over DYE-2, JAR 1, Swiss Camp, Humboldt, and Tunu-N AWS sites, are shown in Figure 7 and are listed in Table 4. In addition, the same statistics are shown for the net radiation, at the JAR 1 AWS site, in Figure 7. (Only a single site is used to evaluate the model net radiation budget, since only the net radiation measurements from the JAR 1 AWS were considered to be reliable, as discussed in section 3.)

The Polar MM5 simulations accurately represent the seasonal evolution of the downwelling shortwave radiation (Figure 7a) but tend to underestimate this quantity with a bias that ranges from -20.4 to -0.8 W m^{-2} (Figure 7b). Biases in the modeled downwelling shortwave radiation may be caused by errors in the modeled clear-sky shortwave transmissivity, cloud cover, or cloud/radiation interactions and need to be explored using detailed cloud and radiation observations. The correlation between the modeled and the observed downwelling shortwave radiation time series is largest during the summer months and smallest during the winter months (0.77 to 0.95). The low-elevation angle of the Sun during the winter months causes increased errors in both the measured and the modeled shortwave radiative fluxes and probably accounts for the reduced correlation at this time of year. The RMSE exhibits a pronounced seasonal cycle, with maximum values during the summer months and minimum values during the winter months. The AWS observations represent an hourly average of the downwelling shortwave radiation for the hour prior to the observation time, while the Polar MM5 radiative fluxes represent instantaneous values at the model output time. This difference in the averaging time of the radiative fluxes causes part of the RMSE evident in Figure 7. (Calculation of the RMSE for hourly averaged and instantaneous samples of idealized annual and daily cycles of the downwelling shortwave radiation indicates a seasonal distribution of the RMSE similar to that shown in Figure 7b, with a maximum value of 55 W m^{-2} during the summer months and a minimum value of 0 W m^{-2} during the winter months). This portion of the error cannot be accounted for in the model / AWS comparison since the model data are only archived at 3 hourly intervals.
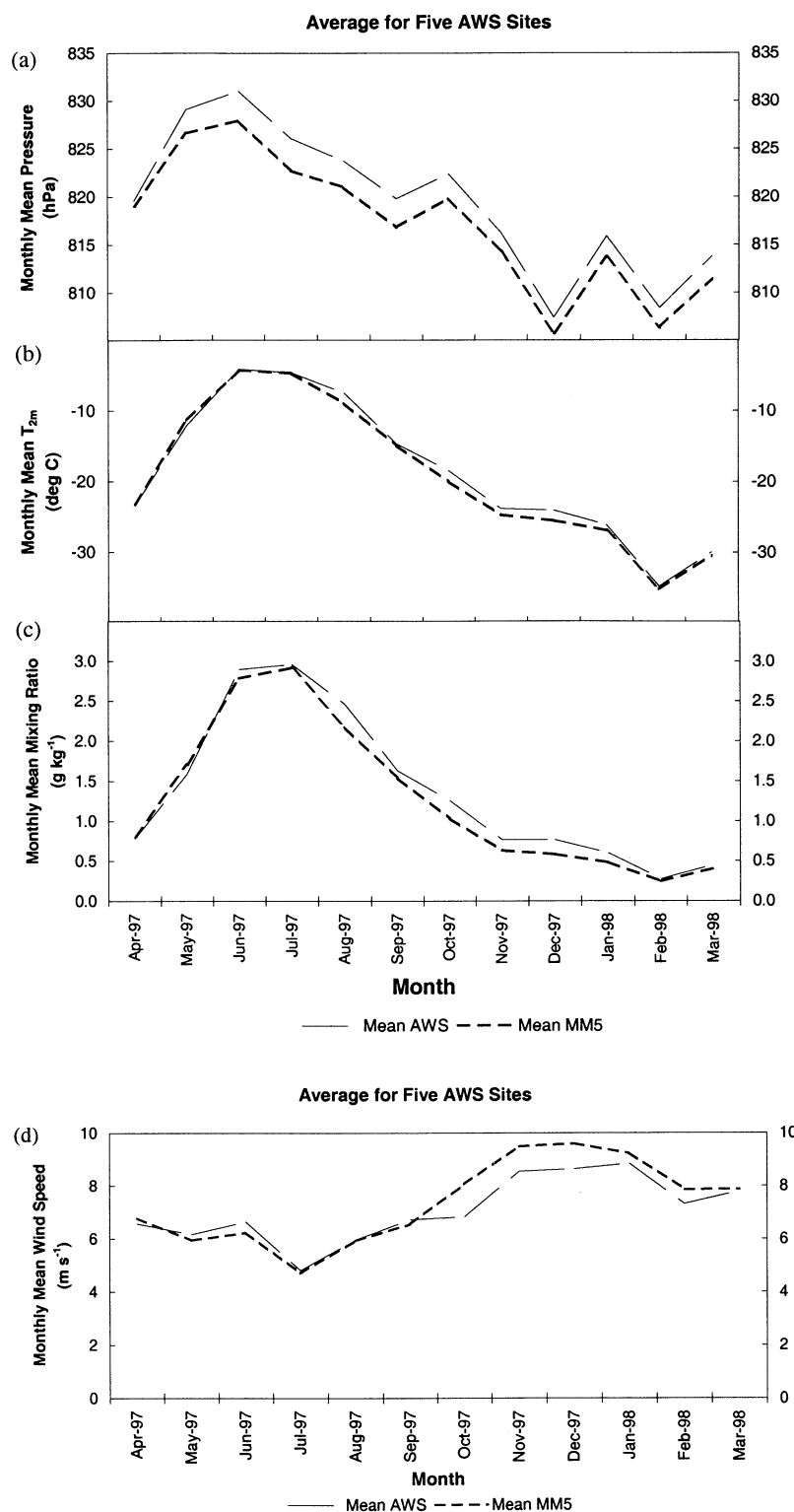
Figure 5. Monthly mean values of pressure (P) (a), air temperature at 2 m (T_{2m}) (b), water vapor mixing ratio (c), and wind speed at 2 m (d) calculated from the Polar MM5 simulations (thick dashed lines) and from the GC-NET AWS observations (thin dashed lines) for April 1997 through March 1998. The monthly mean values have been averaged over five AWS sites (and model grid points) as described in the text.

From Figures 7c and 7d it is evident that the Polar MM5 simulations significantly underestimate the net radiation at the JAR 1 AWS site during the summer months but adequately represent the net radiation during the remainder of the year. The magnitude of the bias in the modeled net radiation budget has maximum values of 40 W m^{-2} during the summer months and is generally less than 20 W m^{-2} for the rest of the year. The negative bias in the net radiation budget that is evident for most months may be caused, in part, by a known error in the CCM2 radiation parameterization that leads to a
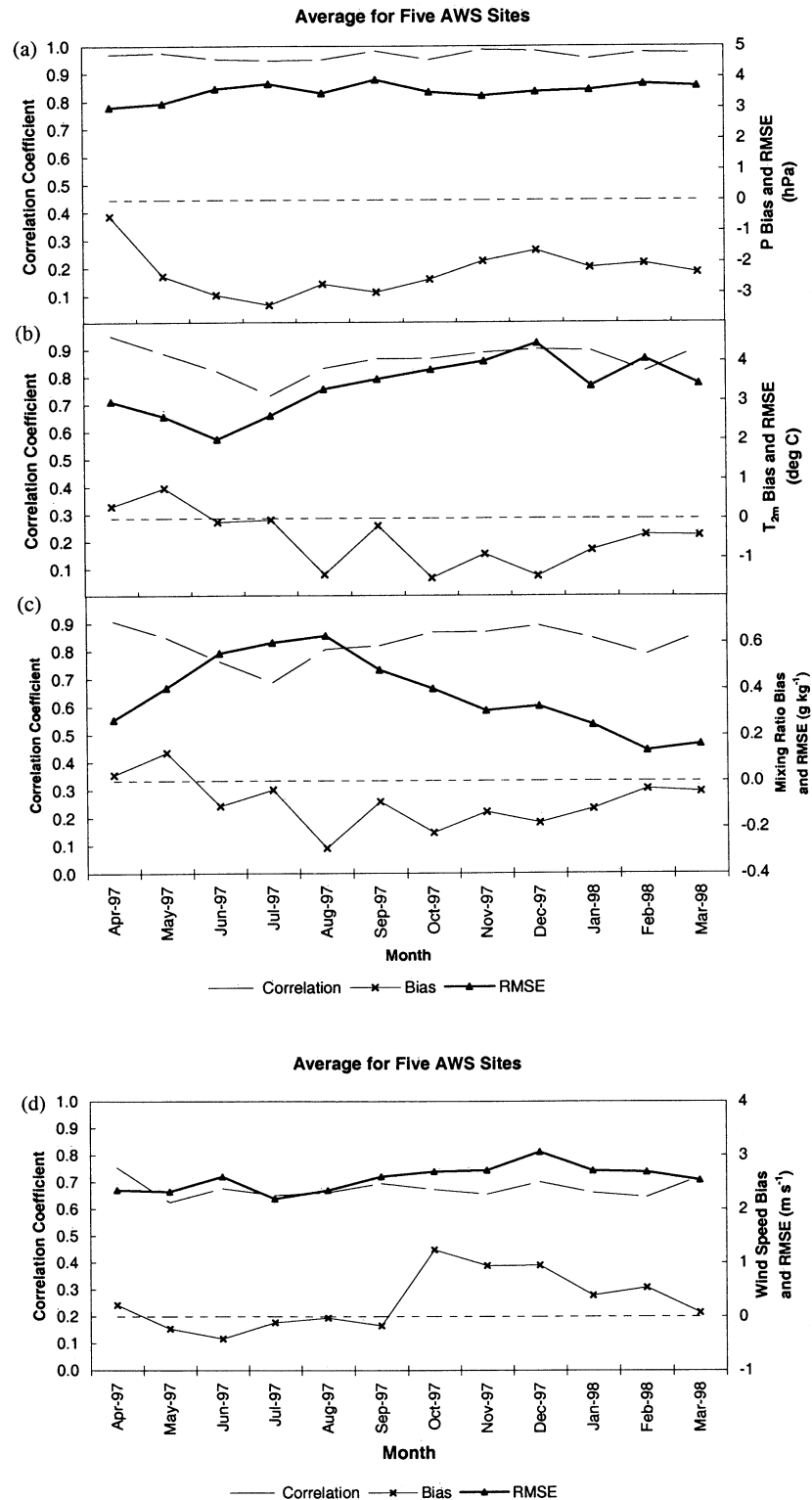
Figure 6. Monthly model verification statistics for pressure (P) (a), air temperature at 2 m (T_{2m}) (b), water vapor mixing ratio (c), and wind speed at 2 m (WS_{2m}) (d) for April 1997 through March 1998. The bias is plotted as a solid line with cross symbols, the root-mean-square error (RMSE) is plotted as a thick solid line with triangles, and the correlation coefficient is plotted as a long-dashed line. The short-dashed line marks the zero bias value. The statistics have been averaged over five AWS sites (and model grid points) as described in the text.

significant underestimation of the downwelling longwave radiation under cold, clear-sky conditions [*Pinto et al.*, 1997].

The large bias during June through August is caused by a combination of the problem with the downwelling longwave radiation in the CCM2 radiation parameterization and by the use of an unrealistically large albedo (0.8) in the model in the ablation zone of the ice sheet. The AWS observations of downwelling and upwelling shortwave radiation indicate that

Table 4. Minimum and Maximum Monthly Average Bias, Root-Mean-Square Error (RMSE), and Correlation Coefficient (Corr.) for Polar MM5 Simulations From April 1997 to March 1998 Averaged for all GC-NET AWS Sites (All), at DYE-2, JAR 1, Swiss Camp, Humboldt, and Tunu-N GC-NET AWS Sites, and Averaged for the Five GC-NET AWS Sites With Complete Data Records (Five)[a]

GC-NET AWS Sites	Pressure			Air Temperature			Mixing Ratio		
	Bias (hPa)	RMSE (hPa)	Corr.	Bias (°C)	RMSE (°C)	Corr.	Bias (g kg⁻¹)	RMSE (g kg⁻¹)	Corr.
All	-2.36 / -0.26	2.91 / 3.71	0.93 / 0.99	-1.61 / 0.81	2.41 / 5.00	0.74 / 0.94	-0.21 / 0.15	0.11 / 0.57	0.70 / 0.91
Five	-3.41 / -0.53	3.01 / 3.91	0.95 / 0.99	-1.53 / 0.77	2.02 / 4.47	0.73 / 0.95	-0.29 / 0.12	0.13 / 0.63	0.69 / 0.91
DYE-2	-2.56 / 1.12	1.79 / 2.93	0.95 / 0.99	-2.68 / -0.16	2.55 / 6.41	0.79 / 0.95	-0.33 / 0.03	0.16 / 0.73	0.74 / 0.97
JAR 1	-3.18 / -1.02	2.12 / 3.50	0.96 / 0.99	-2.00 / 0.44	1.79 / 3.45	0.68 / 0.96	-0.58 / 0.04	0.22 / 0.87	0.67 / 0.93
Swiss Camp	-2.65 / 0.21	1.94 / 3.04	0.96 / 0.99	-0.34 / 1.93	1.50 / 3.61	0.71 / 0.97	-0.28 / 0.15	0.19 / 0.66	0.69 / 0.95
Humboldt	-0.93 / 2.33	1.43 / 2.99	0.94 / 0.99	-1.35 / 1.30	2.37 / 4.40	0.71 / 0.95	-0.16 / 0.20	0.05 / 0.66	0.61 / 0.93
Tunu-N	-9.18 / -5.28	5.99 / 9.31	0.86 / 0.99	-3.81 / 1.10	1.66 / 5.49	0.68 / 0.95	-0.16 / 0.21	0.05 / 0.51	0.57 / 0.92

Table 4. (continued)

GC-NET AWS Sites	Wind Speed			SWD		
	Bias (m s^{-1})	RMSE (m s^{-1})	Corr.	Bias (W m^{-2})	RMSE (W m^{-2})	Corr.
All	0.10 / 1.81	2.34 / 3.33	0.55 / 0.75	-14.17 / 12.95	2.68 / 95.58	0.86 / 0.96
Five	-0.41 / 1.24	2.19 / 3.06	0.62 / 0.75	-20.42 / -0.77	2.83 / 85.58	0.77 / 0.95
DYE-2	-1.45 / 1.56	2.34 / 4.07	0.54 / 0.89	-20.93 / 10.52	5.56 / 77.65	0.77 / 0.98
JAR 1	-1.38 / 1.23	2.17 / 3.20	0.54 / 0.77	-40.73 / -0.66	1.19 / 117.74	0.79 / 0.97
Swiss Camp	-1.32 / 1.27	2.22 / 3.21	0.53 / 0.71	-34.84 / -1.19	1.73 / 109.55	0.85 / 0.93
Humboldt	0.84 / 2.37	1.65 / 3.60	0.37 / 0.83	-24.41 / 8.97	4.88 / 80.23	0.80 / 0.96
Tunu-N	-0.04 / 2.21	1.66 / 5.49	0.68 / 0.95	-12.75 / 10.45	3.20 / 82.16	0.40 / 0.95

[a]Values listed in table are given as minimum / maximum

the monthly albedo at the JAR 1 AWS site is as low as 0.7, with some daily values as low as 0.5 during the summer months. The observed reduction in the albedo is caused by melting of the ice surface and leads to increased absorption of downwelling shortwave radiation and an increase in the net radiation budget that is not captured by the Polar MM5 simulations. It should be noted that the albedo derived from the GC-NET AWS measurements at all of the other AWS locations, except Swiss Camp AWS, have monthly mean values close to 0.8 to 0.9 throughout the entire annual cycle.

Given the larger error in the modeled net radiation budget at JAR 1 AWS site during the summer months it is surprising that other model variables do not reflect this error (particularly the modeled air temperature). The forecast mode simulations for July 1997 were rerun using an albedo of 0.7 for all ice sheet grid points with an elevation of less than 1200 m, while keeping all other model conditions identical to explore the model sensitivity to the specified albedo in the ablation zone of the ice sheet. Table 5 lists the model biases for the pressure, temperature, wind speed, and net radiation for the original and the reduced albedo July 1997 simulations at the JAR 1 AWS site. Only the bias in the net radiation exhibits a large change between the pairs of simulations and decreases in magnitude from -30.7 W m^{-2} to -9.5 W m^{-2} for the reduced albedo simulation. The apparent insensitivity of the other near-surface variables to the reduced albedo is caused by the fact that the ice sheet surface during this period is melting, and thus the ice surface temperature is constrained to a maximum of 0°C in both the real world and the model simulations. The increase in the net radiation at the surface for the reduced albedo simulation, and in reality, goes toward melting of the ice surface. The turbulent surface fluxes, which couple the atmosphere and the underlying surface, show little sensitivity because they are dependent on the difference between the surface temperature and the air temperature,

which do not change between the simulations. Without a significant change in the surface temperature the turbulent fluxes do not change, and the overlying atmosphere does not respond to the decreased albedo. The use of an unrealistically large albedo in the ablation zone of the model would impact calculations of the ice sheet melt rate and the evolution of the snow/ice temperature profile. Given the insensitivity of the atmospheric circulation to the erroneously specified albedo, all further discussion will refer to the original simulations with a constant albedo of 0.8.

The correlation coefficient between the modeled and the observed net radiation is smaller than for the other variables considered in this paper but is generally greater than 0.4. The RMSE exhibits a pronounced annual cycle, with a maximum during the summer months. This maximum is caused by the large errors introduced by the overly large albedo in the Polar MM5 during this period and is also a reflection of the different averaging time for the AWS observations and the model output (as discussed above in the context of the downwelling shortwave radiation).

4.3. Synoptic Variability

The synoptic variability in the model simulations is evaluated by considering monthly time series of the 3 hourly AWS observations and the Polar MM5 output. The monthly time series of surface pressure, near-surface air temperature, wind speed, wind direction, and mixing ratio for the JAR 1 and the Humboldt AWS sites for July 1997 and January 1998 are presented in Figures 8 and 9, respectively. These sites were selected for this analysis because they are representative of the model skill at the other AWS sites (Table 4) and provide an evaluation of the model over a range of environments on the Greenland ice sheet (JAR 1, low elevation, west central Greenland; Humboldt, high elevation,

northwestern Greenland). The months of July and January have been selected for further analysis to provide a contrast between the two extreme months of the annual cycle. Also, the model skill (as determined by the correlation coefficients shown in Figure 6) during January 1998 is similar to that for most other months during the 12 month period of the model simulations, while the model skill during July 1997 is generally worse than found for the other months.

For the surface pressure, most of the variability at both sites is well represented by the Polar MM5 (Figures 8 and 9). A negative bias is evident in the surface pressure at JAR 1, during July 1997. The model pressure increases relative to the observed pressure between July 1997 and January 1998 at both sites, as discussed in the seasonal cycle section above. The timing of some of the pressure maxima (minima) in the model time series differs slightly from the observations, although no consistent phase lag is apparent. The excellent agreement between the modeled and the observed pressure time series is consistent with the high monthly correlation of the modeled and observed pressure (Table 4).

During July 1997 the diurnal cycle of the temperature dominates the temperature variability in the observations and the model simulations (Figure 8) and will be discussed below. There is little synoptic scale variability in the observed temperature at JAR 1, while the Polar MM5 indicates slightly

more variability (Figure 8b). At the Humboldt site there is a more pronounced synoptic variability in the observed temperature time series, which is well represented by the Polar MM5 simulations (Figure 8g), although from July 14-18 and 22-24, 1997, the Polar MM5 does not forecast as large a decrease in temperature as was observed (see section 4.4 for further discussion on the source of this problem).

During January 1998 the synoptic variability dominates the variability in the monthly temperature time series at both sites (Figures 9b and 9g). During this month the model accurately represents this synoptic variability, particularly at JAR 1. During the first 10 days of January the modeled time series at Humboldt does not agree with the observations as well as at later times during the month.

The Polar MM5 simulations capture much of the synoptic variability in the observed wind speed during both months (Figures 8 and 9). In addition, the maximum and minimum wind speeds are also accurately represented by the model, although there are some differences in the details of the observed and modeled time series. During July 1997 the wind speed exhibits a diurnal cycle, superimposed on the synoptic timescale variations (Figures 8c and 8h).

The wind direction at both JAR 1 and Humboldt is accurately depicted by the model during January 1998 (Figures 9d and 9i), although a slight bias in the wind
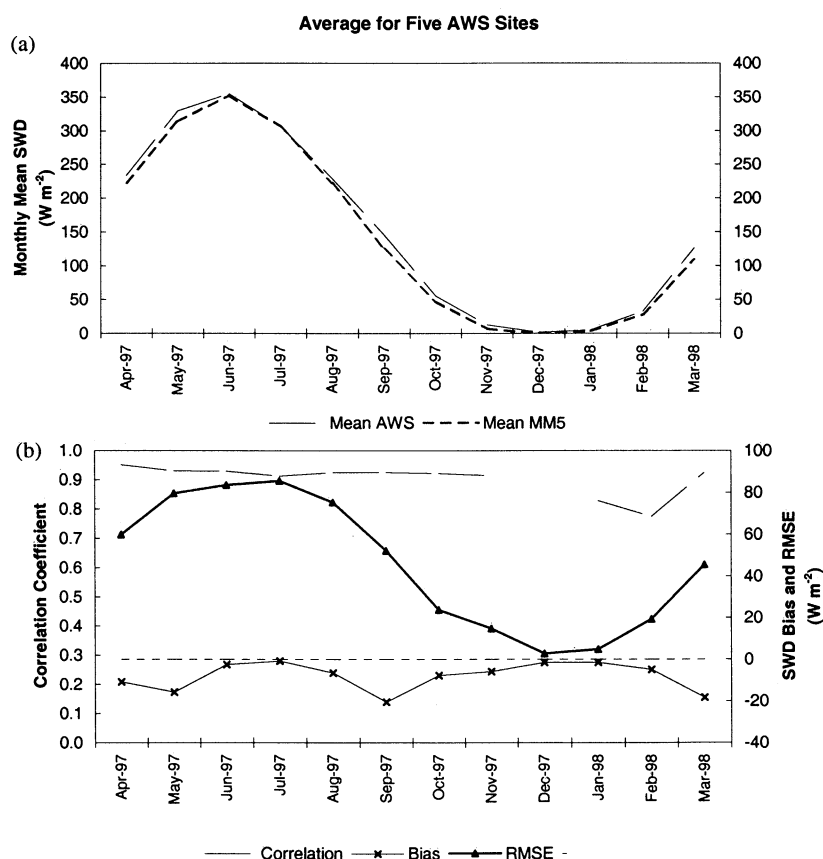
Figure 7. Monthly mean downwelling shortwave radiation (SWD) (a) and monthly mean net radiation (c) calculated from the Polar MM5 (thick dashed line) and from the GC-NET AWS observations (thin dashed line). Monthly model verification statistics (bias, thin line with crosses; root-mean-square error (RMSE), thick solid line with triangles; correlation coefficient, long-dashed line) for the downwelling shortwave radiation (b) and net radiation (d). The zero bias value is plotted as a short-dashed line in Figures 7b and 7d. In Figures 7a and 7b the downwelling shortwave radiation is averaged over five AWS sites (and model grid points) as described in the text. In Figures 7c and 7d the net radiation is for the JAR 1 AWS site only.
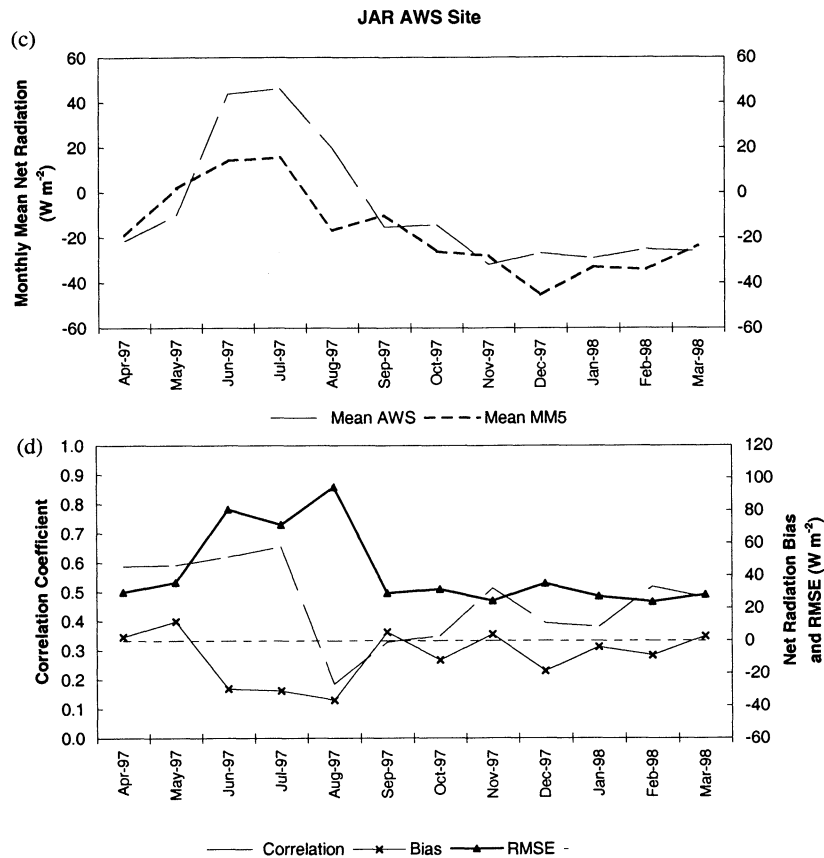
Figure 7. (continued)

direction is evident at JAR 1. During July the observed wind direction is more variable than in January (Figures 8d and 8i). The simulations slightly underestimate this variability at Humboldt but overestimate it at JAR 1. The larger differences in the wind direction at JAR 1 are not surprising given the generally weak wind speeds that are both observed and modeled at this site during July.

During July the modeled and observed mixing ratio exhibits a pronounced diurnal cycle superimposed on the synoptic variations (Figures 8e and 8j). On the synoptic timescale, many of the significant variations in the mixing ratio are depicted by the model simulations. Some of the errors in the modeled mixing ratio time series, particularly during July, mirror the errors in the modeled temperature time series (e.g., July 23-24, 1997, at JAR 1), indicating the importance of accurate temperature forecasts for accurate representation of the atmospheric water vapor. During January the model captures the timing of most of the maxima in the observed mixing ratio time series (Figures 9e and 9j), although consistently underestimates the maximum mixing ratio at JAR 1.

The modeled and AWS-observed downwelling shortwave radiation at JAR 1 and Humboldt for July 1997 are plotted in Figure 10. The time series of the downwelling shortwave radiation is dominated by the diurnal cycle but is modulated by synoptic variability in the cloud cover. For many of the days, the modeled and observed downwelling shortwave radiation are in good agreement. On July 2-4, 7, 21-22, 25-26, and 28-29 the model underestimates the downwelling shortwave radiation, while on July 9-11 and 30, the model

overestimates the downwelling shortwave radiation at JAR 1 (Figure 10a). At Humboldt the model underestimates the downwelling shortwave radiation on July 5, 7, 9, and 14 and overestimates it on July 10-11 and 25 (Figure 10b). These differences between the modeled and the observed downwelling shortwave radiation are probably caused by errors in the model-predicted cloud cover and its radiative effects. On the basis of the larger number of days when the modeled downwelling shortwave radiation is smaller than the observed downwelling shortwave radiation at JAR 1, it appears that the Polar MM5 is simulating excessive cloud cover at this site. No consistent bias in the modeled cloud cover is evident at Humboldt. It is encouraging to note that the model appears to accurately represent the radiative effects of the cloud cover on a number of days during the month, at both sites, when the downwelling shortwave radiation is much

Table 5. Monthly Mean Bias of the Pressure, Temperature, Mixing Ratio, Wind Speed, and Net Radiation for the Control and Reduced Albedo July 1997 Simulations at the JAR 1 AWS Site

Variable	Control	Reduced Albedo
Pressure (hPa)	-3.18	-3.18
Air temperature (°C)	-0.69	-0.69
Mixing ratio (g kg^{-1})	-0.20	-0.16
Wind speed (m s^{-1})	-0.68	-0.73
Net radiation (W m^{-2})	-30.67	-9.52
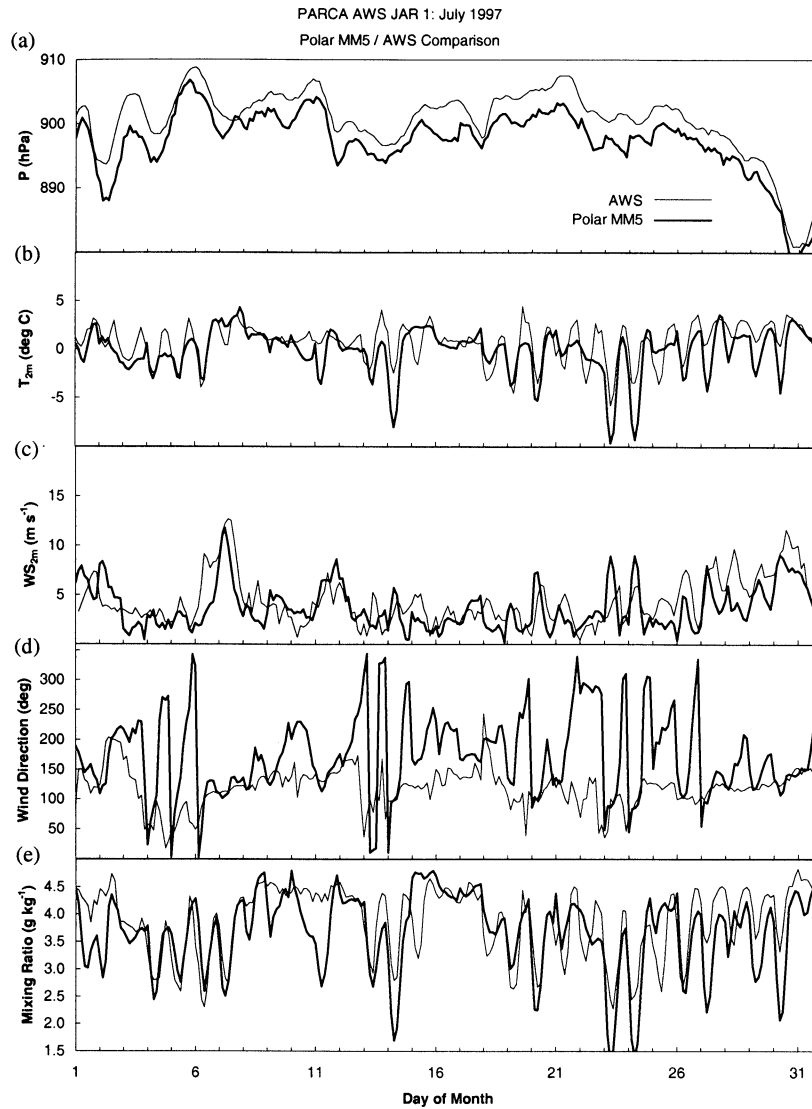
Figure 8. Monthly time series of 3 hourly AWS (thin solid line) and Polar MM5 (thick solid line) data at JAR 1 AWS (Figures 8a-8e) and Humboldt AWS (Figures 8f-8j) for July 1997. The pressure (P) is plotted in Figures 8a and 8f), the air temperature at 2 m (T_{2m}) is plotted in Figures 8b and 8g, the wind speed at 2 m (WS_{2m}) is plotted in Figures 8c and 8h, the wind direction is plotted in Figures 8d and 8i, and the water vapor mixing ratio is plotted in Figures 8e and 8j.

less than the expected clear-sky amount (e.g., July 15-17 at JAR 1 and July 26-28 at Humboldt).

The monthly time series of the modeled and observed net radiation and model-predicted cloud fraction at JAR 1 for July 1997 and January 1998 are shown in Figure 11. The modeled net radiation for the reduced albedo Polar MM5 simulations for July 1997 are also plotted in Figure 11a. During July 1997 the model consistently underestimates the daily maximum in the net radiation at JAR 1 (Figure 11a) as a result of the difference between the fixed albedo used in the model and the much lower albedo observed at this site during periods of melting. The errors in the net radiation at JAR 1, during July 1997 are largest during periods of reduced cloud cover (as inferred from the maximum values of downwelling shortwave radiation in Figure 10), when the error in the model-specified albedo has the largest effect. The modeled net radiation for the reduced albedo simulations shows better agreement with

the daily maximum of the observed net radiation values but still underestimates this quantity on a number of days (July 12-14 and 22-29). This underestimation is caused by errors in the modeled cloud cover and periods when the observed albedo is as small as 0.5. The errors in the net radiation budget could be avoided in future simulations with the use of a prognostic albedo in the model.

During January 1998 the net radiation budget (Figure 11c) is dominated by the longwave radiation budget. Changes in cloud cover (optical thickness, cloud base temperature, etc.) can significantly alter the net radiation budget, and minima in the net radiation time series are likely to be associated with clear-sky (or thin cloud) conditions. Overall, the modeled and observed net radiation time series agree reasonably well, particularly considering the problems associated with accurately predicting cloud cover and cloud radiative effects in mesoscale models. Periods when the modeled and observed
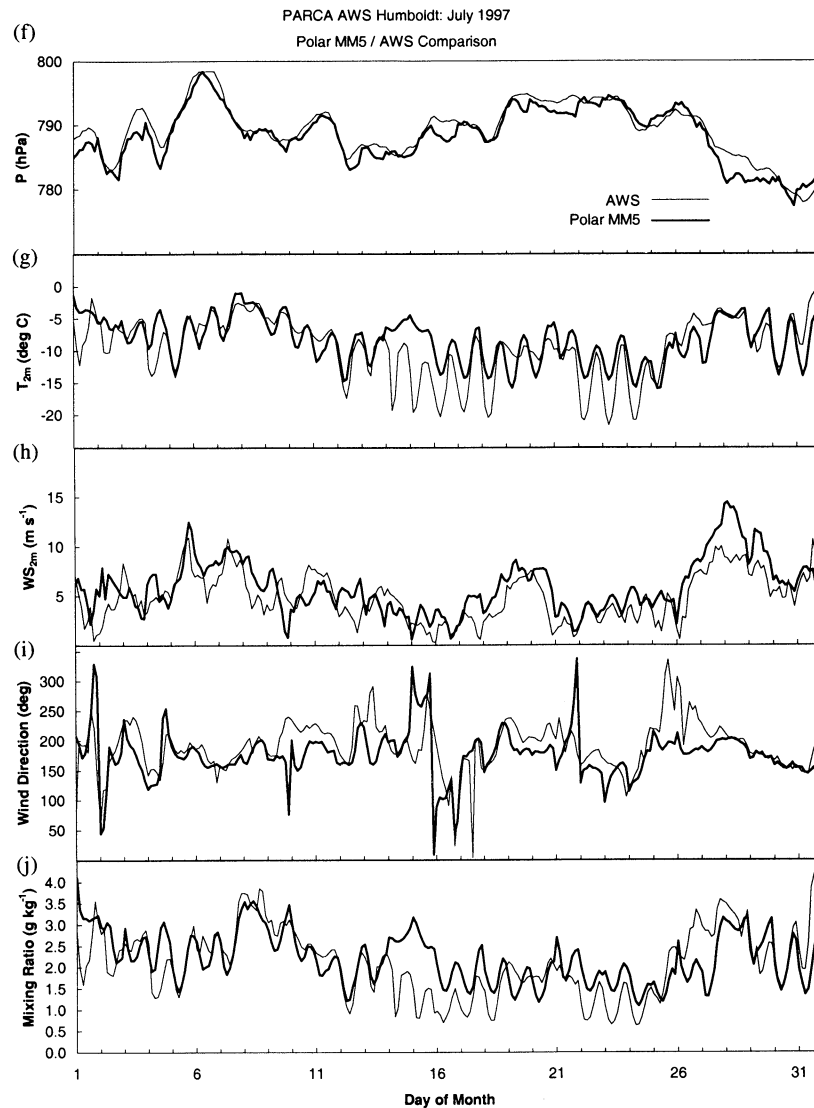
Figure 8. (continued)

net radiation budgets do not match are probably caused by errors in the simulated cloud cover and its radiative properties (Figures 11c and 11d). As an example, during the period from January 7-10, 1998, the Polar MM5 net radiation is 40 W m^{-2} greater than the observed net radiation. Also, during this period the Polar MM5 simulates persistent overcast conditions that are probably in error. The alternate situation also occurs, where the Polar MM5 fails to accurately predict the presence of clouds and thus underestimates the net radiation (e.g., January 25, 1998).

4.4. Diurnal Cycle

The average diurnal cycle for selected variables is calculated for each month as the monthly averaged departure from the daily mean at each observation time for each data set (3 hourly AWS observations or MM5 output) separately. The average diurnal cycle of temperature, water vapor mixing ratio, wind speed, and zonal and meridional wind components at JAR 1 and Humboldt for July 1997 is shown in Figure 12, with the standard error plotted as error bars for each 3 hourly observation (or model output) time.

At both JAR 1 and Humboldt the Polar MM5 reproduces the mean diurnal cycle of air temperature quite accurately, and the observed and modeled diurnal cycles are not statistically different (based on the error bars in Figures 12a and 12e). At JAR 1 the AWS observations indicate a slightly larger diurnal temperature range than forecast by the Polar MM5 (Figure 12a). This larger diurnal temperature range is not unexpected given the larger diurnal amplitude of the net radiation budget (as discussed in section 4.3 and below). At Humboldt the AWS observations also exhibit a larger diurnal temperature range than is forecast by the model (Figure 12e). This difference is due primarily to incorrect forecasts of the minimum temperature during the periods July 14-18 and 22-24 (Figure 8g). During July 14-16 the Polar MM5 predicts overcast conditions (not shown), which limit cooling during the low Sun period of the day, and results in an overestimation of the daily minimum temperature. During the remaining days when the Polar MM5 simulates overly warm minimum temperatures the modeled and observed wind speeds are light (generally less than 3 m s^{-1}). During this period the ground temperature simulated by the Polar MM5
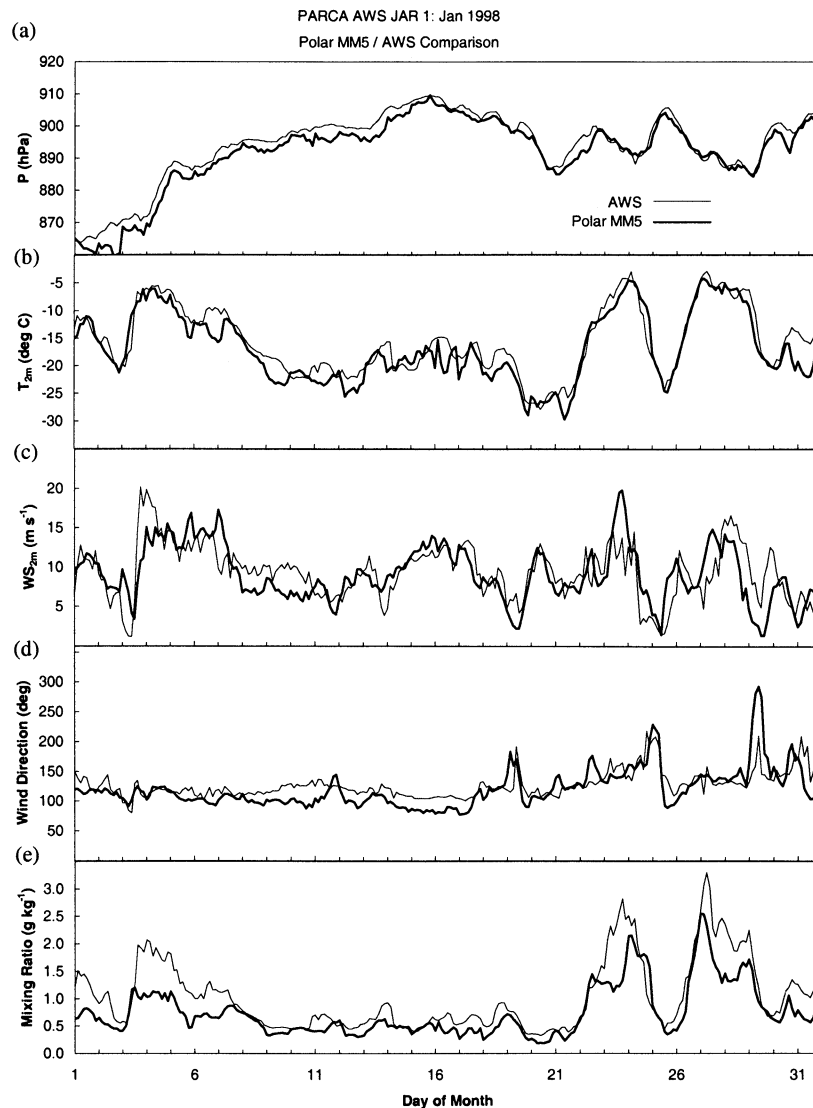
Figure 9. Same as Figure 8 except that data plotted are for January 1998.

closely matches the AWS observed air temperature (not shown), and this is indicative of an error in the coupling of the atmosphere and the surface under statically stable, light wind conditions in the model surface layer parameterization. This problem is also evident at other AWS sites during periods of light winds and clear-sky conditions.

The Polar MM5-simulated average diurnal cycle of the water vapor mixing ratio also closely matches the observed diurnal cycle of this variable and is not statistically different from the observed diurnal cycle (Figures 12b and 12f). Differences between the modeled and the observed diurnal cycle of the water vapor mixing ratio are qualitatively similar to the errors in the modeled diurnal temperature cycle. As discussed above, accurate forecasts of the low-level moisture content of the atmosphere require an accurate prediction of the near-surface air temperature.

A pronounced diurnal cycle in the near-surface wind speed, with a maximum during the period of minimum air temperature is evident in the Polar MM5 simulations (Figures 12c and 12g). This behavior is consistent with primarily katabatically forced winds. The AWS observations at JAR 1

and Humboldt also indicate a pronounced diurnal cycle in the observed wind speeds, although of slightly smaller amplitude and with a 3 to 6 hour lag relative to the Polar MM5 simulations, and the observed minimum air temperature. Other observations of the diurnal cycle of katabatic winds in Greenland and the Antarctic indicate a similar lag in the maximum wind speed relative to the minimum air temperature [*Wendler et al.,* 1988; *van den Broeke,* 1996; *Heinemann,* 1999]. This lag has been attributed to a "time lag required for the gravity-driven wind to react to changes in the inversion strength" [*Wendler et al.,* 1988] and to "the inertial response of the wind field to the thermal forcing" [*van den Broeke,* 1996]. An alternate explanation may involve the turbulent mixing of higher momentum air from the elevated katabatic jet to the surface as the near-surface stability begins to decrease (as the air temperature increases). This mixing becomes increasingly important as the daytime heating progresses, but the diurnal decay of the katabatic jet causes the maximum wind speed at the surface to occur at a time intermediate between the coldest temperature, and strongest katabatic flow aloft, and the warmer daytime temperatures,
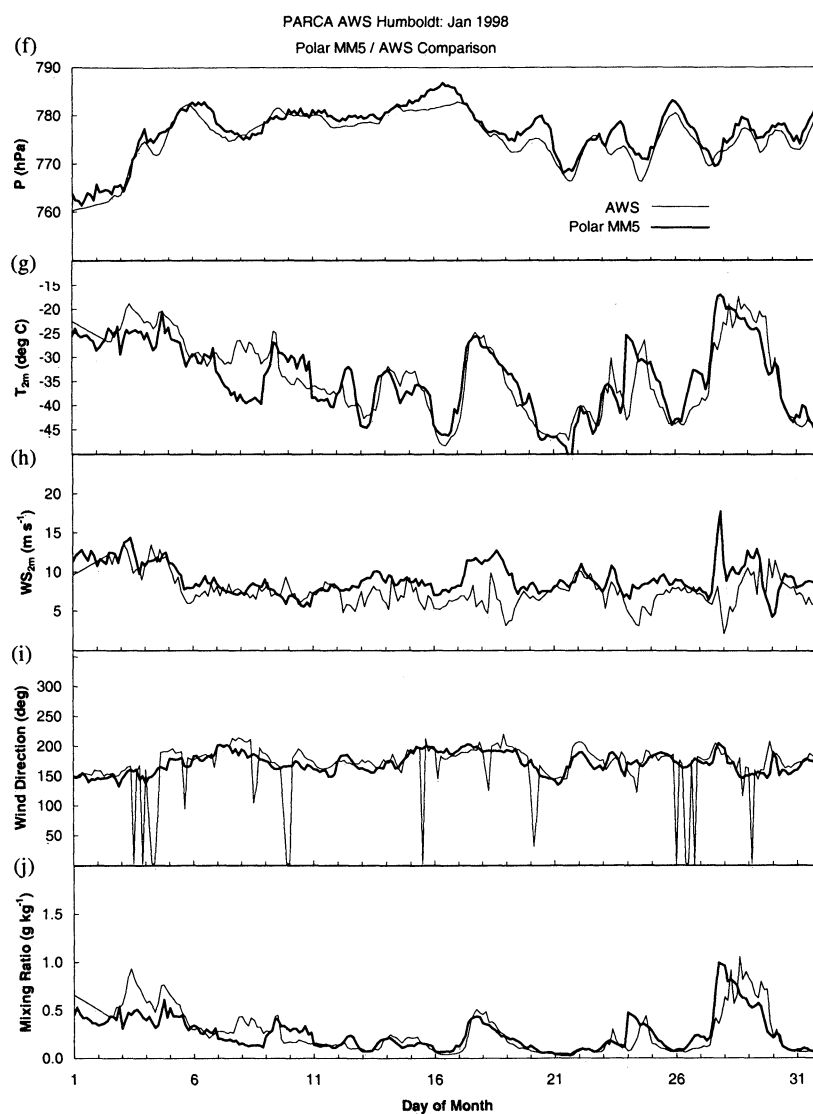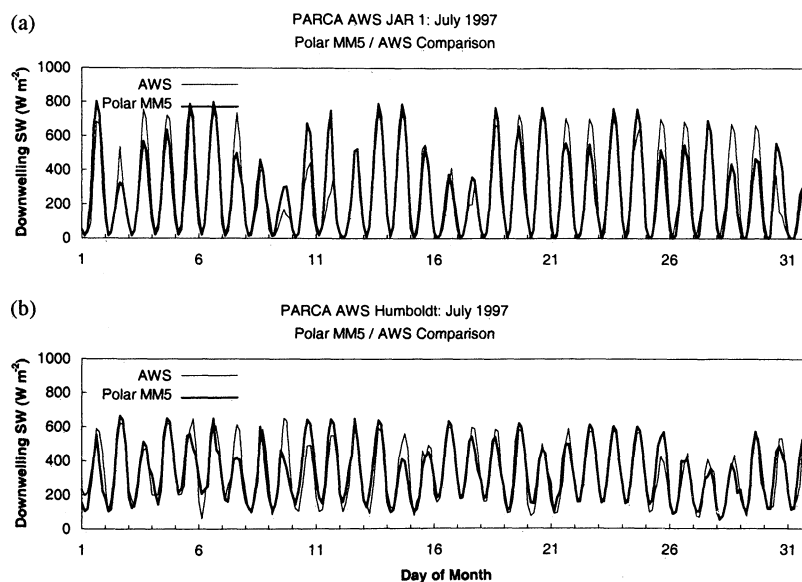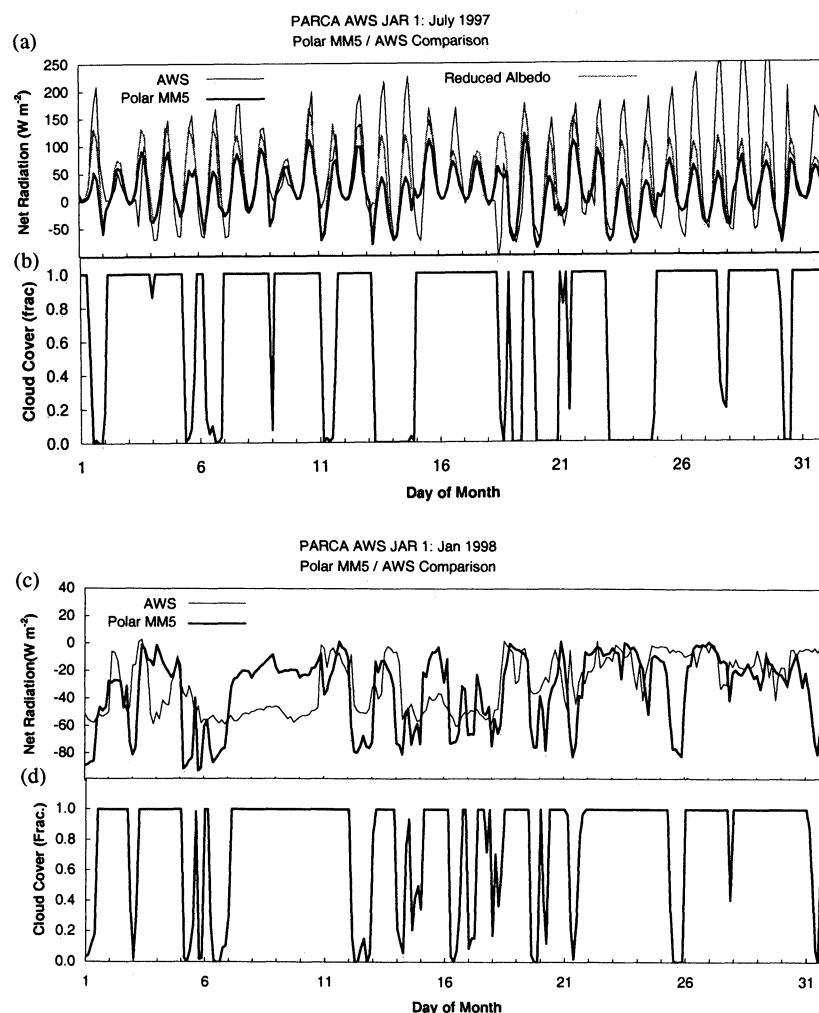
Figure 9. (continued)

Figure 10. Monthly time series of 3 hourly AWS (thin solid line) and Polar MM5 (thick solid line) downwelling shortwave (SW) radiation at JAR 1 (a) and Humboldt (b) AWS sites for July 1997.

Figure 11. Monthly time series of 3 hourly AWS (thin solid line) and Polar MM5 (thick solid line) data at JAR 1 AWS for July 1997 (Figures 11a and 11b) and January 1998 (Figures 11c and d). The modeled and observed net radiation is plotted in Figures 11a and 11c and the modeled fractional cloud cover is plotted in Figures 11b and 11d. The Polar MM5 net radiation for the reduced albedo simulations is plotted as a thick, gray line in Figure 11a.

and enhanced turbulent coupling of the surface winds to the elevated katabatic jet. This process would require a very accurate, and high resolution, representation of the boundary layer over the ice sheet for accurate depiction of the diurnal cycle of the wind speed in a numerical model, and may explain the failure of the Polar MM5 to represent the delay in peak surface wind speed relative to the minimum air temperature.

The observed and modeled diurnal cycle of the zonal and meridional wind components are shown in Figures 12d and 12h (note that at JAR 1 an increase in downslope flow corresponds to a decease in the zonal wind component (i.e., increasingly easterly flow) and at Humboldt an increase in the downslope flow corresponds to an increase in the meridional wind component and a decrease in the zonal wind component). At JAR 1 the modeled and observed diurnal cycles of the meridional wind components are nearly identical and have a similar phase. The modeled zonal wind component has a larger diurnal amplitude than the observations, and both the modeled and the observed zonal wind components have a

minimum value (maximum downslope flow) (Figure 12d) which corresponds to the time of maximum wind speed (Figure 12c). The differences in the amplitude and phase of the modeled and observed diurnal cycle of the zonal wind components lead to the large differences between the modeled and the observed wind direction at JAR 1 (Figure 8d). At Humboldt the observed and modeled diurnal cycle of the zonal wind have a similar phase, with the modeled diurnal cycle having a slightly larger amplitude (Figure 12h). Both the modeled and the observed time of the maximum meridional wind corresponds to the time of the maximum wind speed at Humboldt (Figures 12g and 12h), with the 6 hour phase lag between the modeled and the observed peak meridional wind speed. At both sites the errors in the timing of the maximum wind speed are found to be caused by errors in the timing of the maximum downslope wind speed. This adds additional support to the supposition that the errors in the timing of the maximum wind speed are related to an error in the representation of the details of the katabatic winds in the relatively coarse vertical resolution Polar MM5.
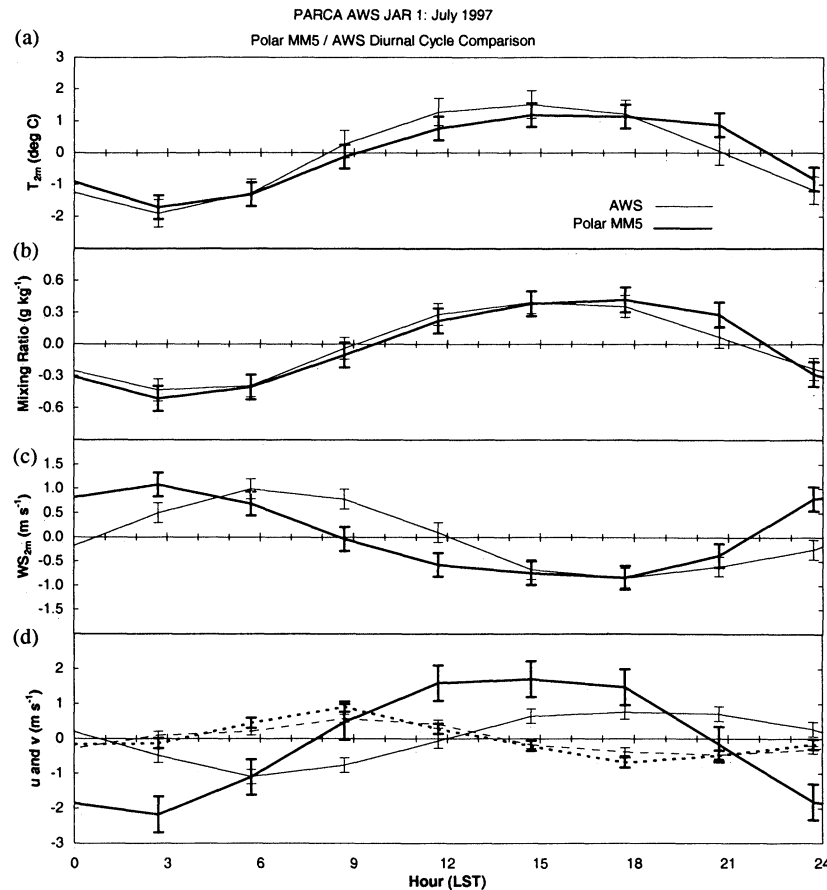
Figure 12. Averaged diurnal cycle calculated from the AWS (thin line) and Polar MM5 (thick line) data at JAR 1 (Figures 12a-12d) and Humboldt (Figures 12e-12h) AWS sites for July 1997. The average diurnal cycle is plotted for the air temperature at 2 m (T_{2m}) in Figures 12a and 12e, for the water vapor mixing ratio in Figures 12b and 12f, for the wind speed at 2 m (WS_{2m}) in Figures 12c and 12g, and for the zonal (u) and meridional (v) wind components in Figures 12d and 12h. The zonal wind is plotted as a solid line and the meridional wind is plotted as a dashed line in Figures 12d and 12h. The standard error is plotted at each observation (model output) time as vertical bars. The data are plotted relative to local standard time (LST) (LST = UTC − 3.3 hours for JAR 1 and LST = UTC − 3.8 hours for Humboldt).

5. Conclusions and Discussion

Results from 12 months of simulations using the Polar MM5, a mesoscale model with physical parameterizations optimized for use over extensive ice sheets, has been presented. A series of daily 48 hour forecasts were performed with the Polar MM5, with the final 24 hours of each forecast used to compile a 12 month data set of model output. Evaluation of the model simulations has primarily used the GC-NET AWS array [*Steffen et al.,* 1996], and has focused primarily on the atmospheric state (pressure, temperature, mixing ratio, wind speed, and wind direction) and limited radiative fluxes (shortwave radiation budget at multiple sites and the net radiation budget at one AWS site).

The model has been found to accurately represent the short-term (48 hour) evolution of the atmosphere for all seasons, with minimal bias in the modeled variables. The Polar MM5 is most skillful in the prediction of the surface pressure and temperature, with slightly less skillful predictions of the water vapor mixing ratio and the winds. For the annual mean the largest error in the model simulations is

excessive precipitation along the steep margins of the Greenland ice sheet.

The modeled downwelling shortwave radiation is in good agreement with the available observations, although the use of a fixed albedo in the model generates sizable errors in the net shortwave radiation budget during periods of melting, when the observed albedo decreases significantly. Evaluation of the net radiation budget was possible at only one AWS site, and the model reproduced the observed net radiation with moderate skill. Large errors in the modeled net radiation were present during the summer as a result of the fixed albedo assumed in the Polar MM5. During the winter the net radiation budget, which is dominated by longwave radiation and cloud-radiation interactions, showed a surprising degree of skill, but evaluation of the model physics with detailed cloud and radiation observations is required.

The modeled and observed diurnal cycles were not statistically different for temperature or water vapor mixing ratio. An error in the timing of the peak wind speed was found in the model. The Polar MM5 predicts maximum wind speeds coincident with the period of minimum air temperature,
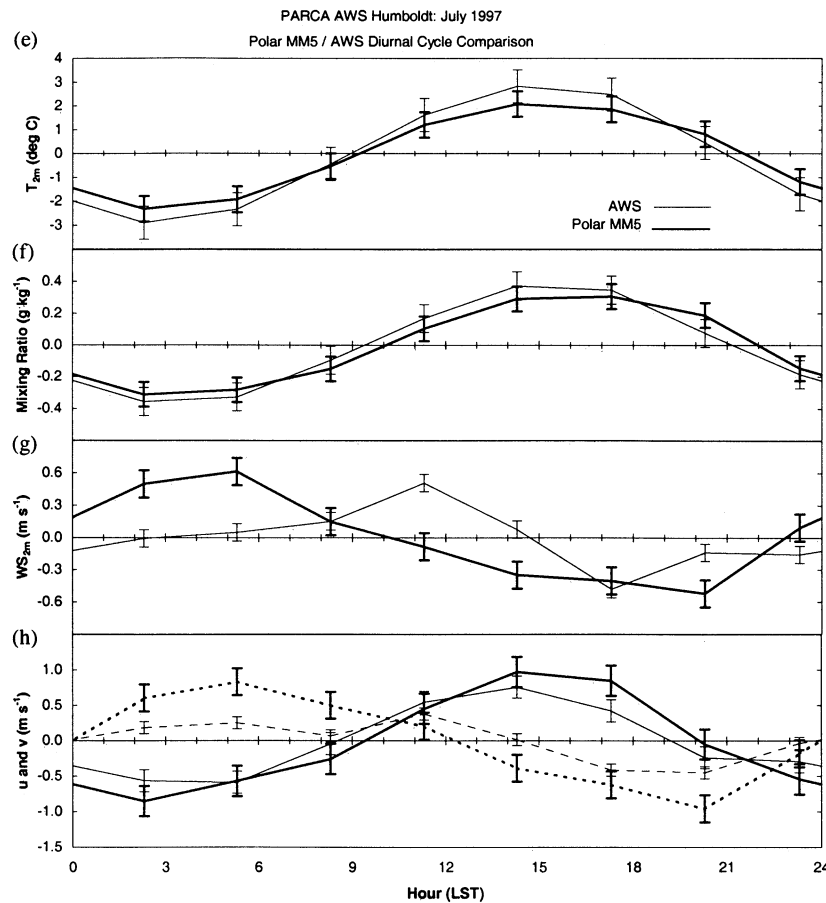
Figure 12. (continued)

indicative of purely katabatic-driven surface winds. The observations indicate a delay in peak wind speed relative to the minimum air temperature and may reflect complex interactions between the near-surface katabatic flow and vertical mixing through the boundary layer.

Additional model evaluation is required. The current study has focused primarily on evaluation of the atmospheric state and has shown that the Polar MM5 accurately reproduces the observed atmospheric conditions. Further analysis of atmospheric processes are required to confirm that these accurate model simulations are achieved through physically correct mechanisms. Additional analysis should focus on cloud properties and radiative effects, the surface energy balance and turbulent fluxes, and the boundary layer structure. This analysis will require a dedicated field program using a combination of surface in situ and remote sensors, airborne observation platforms, and satellite observations, as is scheduled for the spring and summer of 2001 on the west slope of the Greenland ice sheet.

Given the high level of skill present in the Polar MM5 simulations over the Greenland ice sheet a number of model applications are possible. In general, the Polar MM5 may be used to provide a self-consistent, high-resolution atmospheric forcing for other models. The model output can be used to study the mass balance of the ice sheet, particularly in the interior regions where the precipitation forecasts are most accurate. Ablation can be calculated from the model output using a degree-day method, or by implementing an explicit ablation model in the Polar MM5 (although this would require

the use of a more realistic albedo in the ablation zone). Additionally, the Polar MM5 forecasts of temperature and precipitation can be used to force an ice sheet model. Aside from process studies, the Polar MM5 can be used in a forecast mode to provide accurate short-range forecasts for field operations on extensive ice sheets and is currently being used for this purpose in support of the U.S. Antarctic Program operations in the Antarctic (model output is available on the World Wide Web at http://polarmet1.mps.ohio-state.edu/ANWP).

References

Bromwich, D.H., F.M. Robasky, R.A. Keen, and J.F. Bolzan, Modeled variations of precipitation over the Greenland ice sheet, *J. Clim., 6,* 1253-1268, 1993.

Bromwich, D.H., Y. Du, and K.M. Hines, Wintertime surface winds over the Greenland ice sheet, *Mon. Weather Rev., 124,* 1941-1947, 1996.

Bromwich, D.H., Q.-S. Chen, Y. Li, and R.I. Cullather, Precipitation over Greenland and its relation to the North Atlantic oscillation, *J. Geophys. Res., 104,* 22,103-22,115, 1999.

Bromwich, D.H., J.J. Cassano, T. Klein, G. Heinemann, K.M. Hines, K. Steffen, and J.E. Box, Mesoscale modeling of katabatic winds over Greenland with the Polar MM5, *Mon. Weather Rev.*, in press, 2001.

Cassano, J.J., and T.R. Parish, An analysis of the nonhydrostatic dynamics in numerically simulated Antarctic katabatic flows, *J. Atmos. Sci., 57,* 891-898, 2000.

Chen, Q.-S., D.H. Bromwich, and L. Bai, Precipitation over Greenland retrieved by a dynamic method and its relation to cyclonic activity, *J. Clim., 10,* 839-870, 1997.

Colle, B.A., K.J. Westrick, and C.F. Mass, Evaluation of MM5 and Eta-10 precipitation forecasts over the Pacific Northwest during the cool season, *Weather Forecasting, 14,* 137-154, 1999.

Dudhia, J., A nonhydrostatic version of the Penn State – NCAR mesoscale model: Validation tests and simulation of an Atlantic cyclone and cold front, *Mon. Weather Rev., 121,* 1493-1513, 1993.

Ebert, E.E., and J.A. Curry, A parameterization of ice cloud optical properties for climate models, *J. Geophys. Res., 97,* 3831-3836, 1992.

Ekholm, S., A full coverage, high-resolution, topographic model of Greenland computed from a variety of digital elevation data, *J. Geophys. Res., 101,* 21,961-21,972, 1996.

Fletcher, N.H., *Physics of Rain Clouds,* Cambridge Univ. Press, New York, 1962.

Gallée, H., and P.G. Duynkerke, Air-snow interactions and the surface energy and mass balance over the melting zone of west Greenland during the Greenland Ice Margin Experiment, *J. Geophys. Res., 107,* 13,813-13,824, 1997.

Gloersen, P., W.J. Campbell, D.J. Cavalieri, J.C. Comiso, C.L. Parkinson, and H.J. Zwally, *Arctic and Antarctic Sea Ice, 1978-1987: Satellite Passive – Microwave Observations and Analysis,* NASA, 1992.

Grell, G.A., J. Dudhia, and D.R. Stauffer, A description of the fifth-generation Penn State/NCAR mesoscale model (MM5), *NCAR Tech. Note, NCAR/TN-398+STR,* Natl. Cent. for Atmos. Res., Boulder, Colo., 1994.

Grenfell, T.C., and S.G. Warren, Representation of nonspherical ice particles by a collection of independent spheres for scattering and absorption of radiation, *J. Geophys. Res., 104,* 31,697-31,709, 1999.

Hack, J.J., B.A. Boville, B.P. Briegleb, J.T. Kiehl, P.J. Rasch, and D.L. Williamson, Description of the NCAR community climate model (CCM2), *NCAR Tech. Note, NCAR/TN-382+STR,* Natl. Cent. for Atmos. Res., Boulder, Colo., 1993.

Heinemann, G., The KABEG'97 field experiment: An aircraft-based study of katabatic wind dynamics over the Greenland ice sheet, *Boundary Layer Meteorol., 93,* 75-116, 1999.

Hines, K.M., D.H. Bromwich, and Z. Liu, Combined global climate model and mesoscale model simulations of Antarctic climate, *J. Geophys. Res., 102,* 13,747-13,760, 1997a.

Hines, K.M., D.H. Bromwich, and R.I. Cullather, Evaluating moist physics for Antarctic mesoscale simulations, *Ann. Glaciol., 25,* 282-286, 1997b.

Hurrell, J.W., Decadal trends in the North Atlantic Oscillation, regional temperatures and precipitation, *Science, 269,* 676-679, 1995.

Janjić, Z.I., The step-mountain eta coordinate model: Further developments of the convection, viscous sublayer, and turbulence closure schemes, *Mon. Weather Rev., 122,* 927-945, 1994.

Kiehl, J.T., J.J. Hack, G.B. Bonan, B.A. Boville, B.P. Briegleb, D.L. Williamson, and P.J. Rasch, Description of the NCAR community climate model (CCM3), *NCAR Tech. Note, NCAR/TN-420+STR,* Natl. Cent. for Atmos. Res., Boulder, Colo., 1996.

Manning, K.W., and C.A. Davis, Verification and sensitivity experiments for the WISP94 MM5 forecasts, *Weather Forecasting, 12,* 719-735, 1997.

McConnell, J.R., E. Mosley-Thompson, D.H. Bromwich, R.C. Bales, and J.D. Kyne, Interannual variations of snow accumulation on the Greenland ice sheet (1985-1996): New observations versus model predictions, *J. Geophys. Res., 105,* 4039-4046, 2000.

Meesters, A., Dependence of the energy balance of the Greenland ice sheet on climate change, *Q. J. R. Meteorol. Soc., 120,* 491-517, 1994.

Meyers, M.P., P.J. DeMott, and W.R. Cotton, New primary ice-nucleation parameterizations in an explicit cloud model, *J. Appl. Meteorol., 31,* 708-721, 1992.

Oerlemans, J., and H.F. Vugts, A meteorological experiment in the melting zone of the Greenland ice sheet, *Bull. Am. Meteorol. Soc., 74,* 355-365, 1993.

Ohmura, A., M. Wild, and A. Bengtsson, A possible change in mass balance of Greenland and Antarctic ice sheets in the coming century, *J. Clim., 9,* 2124-2135, 1996.

Parish, T.R., and K.T. Waight, The forcing of Antarctic katabatic winds, *Mon. Weather Rev., 115,* 2214-2226, 1987.

Pinto, J.O., J.A. Curry, and C.W. Fairall, Radiative characteristics of the Arctic atmosphere during spring as inferred from ground-based measurements, *J. Geophys. Res., 102,* 6941-6952, 1997.

Reisner, J., R.M. Rasmussen, and R.T. Bruintjes, Explicit forecasting of supercooled liquid water in winter storms using the MM5 mesoscale model, *Q. J. R. Meteorol. Soc., 124,* 1071-1107, 1998.

Stearns, C.R., G.A. Weidner, and L.M. Keller, Atmospheric circulation around the Greenland crest, *J. Geophys. Res., 102,* 13,801-13,812, 1997.

Steffen, K., and J. Box, Surface climatology of the Greenland ice sheet: Greenland Climate Network 1995-1999, *J. Geophys. Res,* this issue.

Steffen, K., J.E. Box, and W. Abdalati, Greenland climate network: GC-NET, in *Special Report on Glaciers, Ice Sheets and Volcanoes,* edited by S.C. Colbeck, *CRREL 96-27,* pp.98-103, Cold Reg. Res. and Eng. Lab., Hanover, N.H., 1996.

Stull, R.B., *An Introduction to Boundary Layer Meteorology,* Kluwer Acad. Press, Norwell, Mass., 1988.

Thompson, S.L., and D. Pollard, Greenland and Antarctic mass balances for present and doubled atmospheric CO_2 from GENESIS Version-2 global climate model, *J. Clim., 10,* 871-900, 1997.

van den Broeke, The Atmospheric Boundary Layer Over Ice Sheets and Glaciers, Ph.D. thesis, Univ. Utrecht, Utrecht, Netherlands, 1996.

van den Broeke, M.R., and H. Gallée, Observations and simulations of barrier winds at the western margin of the Greenland ice sheet, *Q. J. R. Meteorol. Soc., 122,* 1365-1383, 1996.

van Loon, H., and J.C. Rogers, The seesaw in the winter temperatures between Greenland and northern Europe, part I, General description, *Mon. Weather Rev., 106,* 296-310, 1978.

Wendler, G., N. Ishikawa, and Y. Kodama, The heat balance of the icy slope of Adelie Land, eastern Antarctica, *J. Appl. Meteorol., 27,* 52-65, 1988.

Yen, Y.C., Review of thermal properties of snow, ice and sea ice, *CRREL Rep. 81-10,* Cold Reg. Res. and Eng. Lab., Hanover, N.H., 1981.

J.E. Box, J.J. Cassano, and K. Steffen, Cooperative Institute for Research in Environmental Sciences, University of Colorado at Boulder, 216 UCB, Boulder, CO 80309-0216, USA. (cassano@cires. colorado.edu)

D.H. Bromwich and L. Li, Polar Meteorology Group, Byrd Polar Research Center, The Ohio State University, 1090 Carmack Road, Columbus, OH 43210, USA.